

1
2
3
4
5
6
7
8
9

Reaction of the C₂H radical with 1-butyne (C₄H₆):
Low temperature kinetics and isomer-specific product detection

10 Satchin Soorkia^a, Adam J. Trevitt^b, Talitha M. Selby^c, David L. Osborn^d, Craig A. Taatjes^d,
11
12 Kevin R. Wilson^c and Stephen R. Leone^{a,e,*}

13
14
15 ^aDepartments of Chemistry and Physics, University of California, Berkeley, California 94720,
16 USA

17
18 ^bSchool of Chemistry, University of Wollongong, New South Wales 2522, Australia

19
20 ^cDepartment of Chemistry, University of Wisconsin – Washington County, West Bend, WI
21 53095, USA

22
23
24 ^dCombustion Research Facility, Mail Stop 9055, Sandia National Laboratories, Livermore, CA
25 94551-0969, USA

26
27
28 ^eChemical Sciences Division, Lawrence Berkeley National Laboratory, 1 Cyclotron Road,
29 Berkeley, CA 94720, USA

30
31
32
33 *On appointment as a Miller Research Professor in the Miller Institute for Basic Research in
34 Science

35
36
37
38 Electronic mail: srl@berkeley.edu
39
40
41
42
43
44
45
46
47
48
49
50
51
52
53
54
55
56
57
58
59
60

Abstract

The rate coefficient for the reaction of the ethynyl radical (C_2H) with 1-butyne ($H-C\equiv C-CH_2-CH_3$) is measured in a pulsed Laval nozzle apparatus. Ethynyl radicals are formed by laser photolysis of acetylene (C_2H_2) at 193 nm and detected *via* chemiluminescence ($C_2H + O_2 \rightarrow CH(A^2\Delta) + CO_2$). The rate coefficients are measured over the temperature range of 74-295 K. The $C_2H + 1$ -butyne reaction exhibits no barrier and occurs with rate constants close to the collision limit. The temperature dependent rate coefficients can be fit within experimental uncertainties by the expression $k = (2.4 \pm 0.5) \times 10^{-10} (T/295 \text{ K})^{-(0.04 \pm 0.03)} \text{ cm}^3 \text{ molecule}^{-1} \text{ s}^{-1}$. Reaction products are detected at room temperature (295 K) and 533 Pa using a Multiplexed Photoionization Mass Spectrometer (MPIMS) coupled to the tunable VUV synchrotron radiation from the Advanced Light Source at the Lawrence Berkeley National Laboratory. Two product channels are identified for this reaction: $m/z = 64$ (C_5H_4) and $m/z = 78$ (C_6H_6) corresponding to the CH_3 - and H-loss channels, respectively. Photoionization efficiency (PIE) curves are used to analyze the isomeric composition of both product channels. The C_5H_4 products are found to be exclusively linear isomers composed of ethynylallene and methyldiacetylene in a 4:1 ratio. In contrast, the C_6H_6 product channel includes two cyclic isomers, fulvene 18(\pm 5)% and 3,4-dimethylenecyclobut-1-ene 32(\pm 8)%, as well as three linear isomers, 2-ethynyl-1,3-butadiene 8(\pm 5)%, 3,4-hexadiene-1-yne 28(\pm 8)% and 1,3-hexadiyne 14(\pm 5)%. Within experimental uncertainties, we do not see appreciable amounts of benzene and an upper limit of 10 % is estimated. Diacetylene (C_4H_2) formation *via* the C_2H_5 -loss channel is also thermodynamically possible but cannot be observed due to experimental limitations. The implications of these results for modeling of planetary atmospheres, especially of Saturn's largest moon Titan, are discussed.

1. Introduction

The ethynyl radical, C_2H , is an important polyatomic radical in the interstellar medium.¹ Its relative abundance is a marker of the carbon richness of its environment, as observed on Saturn's largest moon, Titan. C_2H radicals are formed in the cold, dense, structured and complex atmosphere of Titan²⁻⁴ by the photolysis (*via* solar radiation) of acetylene.⁵ Moreover, ethynyl radicals are believed to play a major role in the molecular weight growth of larger carbonaceous species. In a model proposed by Wilson and Atreya,⁶ to account for the dense haze observed on Titan, the reaction of the C_2H radical with acetylene is a key step in the formation of longer chain polyynes molecules (e.g. C_4H_2 and C_6H_2). These polyynes can subsequently react further with C_2H radicals to eventually form much larger polymeric species that ultimately contribute to the observed photochemically active and colored organic haze.⁷ Similarly, C_2H is a key radical in the formation of polycyclic aromatic hydrocarbons (PAHs),⁶ which are believed to play an important role in interstellar chemistry.^{8,9}

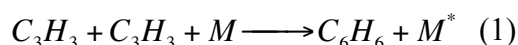
Benzene (C_6H_6), the simplest aromatic hydrocarbon, is considered to be a precursor for larger PAH formation and its recent identification on Titan¹⁰ strongly suggests that much more complex PAH synthesis may proceed in the cold atmosphere of the Saturnian moon. Recently, Mebel and coworkers¹¹ proposed a novel Ethynyl Addition Mechanism (EAM) as a viable alternative to the high-temperature Hydrogen-Abstraction- C_2H_2 -Addition (HACA)¹² mechanism for the formation of PAHs at very low temperatures. As described,¹¹ this mechanism is initiated by the addition of a C_2H radical to an ortho-carbon of ethynylbenzene ($C_6H_5-C\equiv C-H$), and the reactive intermediate subsequently loses a H atom to form 1,2-diethynylbenzene. The latter then reacts with a second C_2H radical *via* addition to one of the carbon atoms on the ethynyl side chains. Ring closure of the intermediate leads to the formation of the ethynyl substituted bicyclic naphthalene core. The authors conclude that since the stepwise addition of C_2H radicals (followed by H atom elimination) to benzene, ethynylbenzene and 1,2-diethynylbenzene occurs without a barrier and with high exothermicity, the reactions of C_2H radicals should be very fast, and they suggest that the reactions should proceed with rate constants on the order of $10^{-10} \text{ cm}^3 \text{ molecule}^{-1} \text{ s}^{-1}$ even at very low temperatures.

1
2
3
4
5 Since C_2H is a key species in carbon-rich environments, it has been the subject of a number of
6 studies.^{11,13-26} In order to analyze and account for the presence of hydrocarbon species, modeling
7 studies are of central importance in understanding the complex nature of Titan's atmosphere.
8 Detailed models have been developed over the last few decades.^{6,27,28} Low temperature rate
9 constants and product branching ratios are used when available to describe accurately and
10 reliably²⁹ the chemical schemes²⁷ that are proposed. In this respect, much progress³⁰ has been
11 made experimentally to obtain kinetic data on key chemical reactions down to very low
12 temperatures relevant to interstellar chemistry. The CRESU (Cinétique de Réaction Chimique en
13 Ecoulement Supersonique Uniforme) technique, pioneered by Rowe and coworkers,^{31,32} involves
14 the expansion of a gas mixture through a Laval nozzle and allows kinetic studies down to 10 K to
15 examine chemistry under true interstellar conditions.³¹⁻³⁵ M. A. Smith and coworkers^{36,37}
16 developed a pulsed Laval apparatus that was adopted by Leone and coworkers²¹ and Abel and
17 coworkers.³⁰ The collimated supersonic flow generated by a Laval nozzle can be compared to a
18 "wall-less flow tube reactor" in which reactions involving species with very low vapor pressures,
19 that otherwise would tend to condense, can be studied. Moreover, the pulsed nozzle produces
20 much less gas flow, requiring lower pumping speeds while yielding rate coefficients that are in
21 satisfactory agreement with continuous flow measurements, as demonstrated in a collaborative
22 work between Leone and coworkers and I. W. M. Smith and coworkers.^{13,25}
23
24
25
26
27
28
29
30
31
32
33
34
35
36
37

38 Although numerous low temperature kinetic measurements of the C_2H radical with C_2 (in this
39 paper, C_n denotes a hydrocarbon species containing n carbon atoms) and C_3 hydrocarbons³⁰ have
40 been performed during the last decade as well as product branching studies,¹⁷ there are, to our
41 knowledge, only a few measurements of rate coefficients with molecules having longer carbon
42 chain lengths (C_4 and higher).^{38,39} As pointed out by Sims and coworkers,³⁸ highly unsaturated
43 hydrocarbon species with four and more carbon atoms tend to be very unstable compounds
44 because, for example, diacetylene polymerizes easily at room temperature. At the same time, the
45 absence of these reactions in photochemical models can lead to underestimates of reaction
46 pathways that otherwise would be non-negligible.⁴⁰ Furthermore, the photolysis of larger
47 molecules may be a source of smaller neutral and radical species.⁴⁰ Therefore, it is suggested that
48 future photochemical models will require including reactions of species containing four or more
49
50
51
52
53
54
55
56
57
58
59
60

1
2
3 carbon atoms, hence taking into account the underlying contributions of higher molecular weight
4 species for more accurate chemical descriptions of Titan's atmosphere in models.
5
6
7

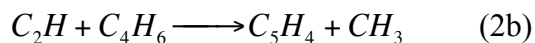
8 A recent study by Vuitton and coworkers⁴¹ provides insight into the formation and distribution of
9 benzene, a C_6 hydrocarbon species, on Titan. The three-body propargyl recombination reaction
10 (see Eq. 1) used in models^{42,43} fails to predict the large mole fractions of benzene observed in the
11 thermosphere on Titan.
12
13
14



15
16
17
18
19
20
21 Indeed, three-body reactions are unlikely at low densities ($\sim 10^{12} \text{ cm}^{-3}$ of N_2 at an altitude of ~ 800
22 km).⁴¹ Considering the time constants of key ion reactions,⁴¹ the authors suggest that benzene in
23 the ionosphere is likely produced by ion-molecule chemistry. The globally averaged column-
24 integrated production rate of benzene in the ionosphere ($\sim 10^7 \text{ cm}^{-2}\text{s}^{-1}$) is found to be of the same
25 order of magnitude as the radical-neutral production rate ($\sim 4 \times 10^6 \text{ cm}^{-2}\text{s}^{-1}$). The radical-neutral
26 ($C_2H + C_4H_6$) and radical-radical ($C_2H_3 + C_4H_3$) reactions are identified as potential reactions to
27 be included in models and the authors strongly emphasized that low temperature rate coefficients
28 and product identification are required for these reactions. Conversely, in a recent combustion
29 study, Hansen and coworkers⁴⁴ showed that C_6H_6 is formed primarily through $C_3H_3 + C_3H_3$ and *i*-
30 $C_4H_5 + C_2H_2$. In flames, the concentration of propargyl radicals is much higher and the formation
31 of benzene *via* this pathway is more favorable. It is therefore of fundamental interest to explore
32 the possible formation reactions of C_6 molecules in the cold, low pressure and photochemically
33 driven atmospheres of the outer planets, and especially Titan.
34
35
36
37
38
39
40
41
42
43
44

45
46 Carbon-containing radicals usually react with unsaturated hydrocarbon species where a short-
47 lived intermediate⁴⁵ is formed and decomposes to give the substituted product, i.e. H-loss channel
48 or CH_3 -loss channel¹⁷ (see Eqs. 2a and 2b). The reaction of C_2H with a C_4 substituted alkyne, 1-
49 butyne (C_4H_6), is one such reaction with the possibility of forming cyclic C_6 molecules, in
50 particular benzene.
51
52
53
54





Indeed, in this study we have identified C_6H_6 as one of the reaction products, corresponding to the H-loss channel according to Eq. 2a. Also, we have identified C_5H_4 consistent with the CH_3 -loss channel as indicated in Eq. 2b. However, in our study the formation of benzene is not observed. The product detection using Multiplexed Photoionization Mass Spectrometry (MPIMS) coupled to tunable VUV synchrotron radiation is intriguing, revealing the presence of cyclic isomers of C_6H_6 other than benzene, as well as linear isomers. In this paper, we first report low temperature rate coefficient measurements for the reaction of the ethynyl radical with 1-butyne over the 74-295 K temperature range in a pulsed Laval nozzle using a chemiluminescence tracer method. The product detection and isomer identification are performed in a slow flow reactor using Multiplexed Photoionization Mass Spectrometry. Time-resolved Photoionization Efficiency (PIE) curves, i.e. the ion signal as a function of the synchrotron photon energy, for the two product channels are measured. The different product isomers appear as distinct thresholds and are identified according to their ionization energies and the shapes of their Franck-Condon profiles. The implications of these results for polyynes formation and their potential role for molecular weight growth chemistry in planetary atmospheres, especially on Titan, are also discussed.

2. Experiment

Two different apparatuses are used to study the reaction of the ethynyl radical (C_2H) with 1-butyne (C_4H_6). First, low temperature kinetic measurements are made in a pulsed Laval nozzle apparatus, followed by isomer-resolved product branching studies using a Multiplexed Photoionization Mass Spectrometer (MPIMS) coupled to tunable VUV synchrotron radiation at the Advanced Light Source at the Lawrence Berkeley National Laboratory. Experimental details such as error bars for the kinetics measurements, signal-to-noise ratio and data collection are also discussed. Calculations using the CBS-QB3 composite method^{46,47} are performed to determine adiabatic ionization energies of C_5H_4 and C_6H_6 isomers relevant to this work. Photoionization energy curves are computed using the PESCAL program of Ervin.^{48,49}

2.1. Low temperature Laval kinetics

The rate coefficients are measured in a pulsed Laval nozzle apparatus using laser photolysis and the chemiluminescence tracer method. A detailed description and schematic of the apparatus has been reported elsewhere.²¹ In this paper, only the main features of the experiment will be presented. The experimental setup consists of a Laval nozzle mounted on a reservoir block under medium vacuum (0.1 – 1.0 Torr maintained by a Leybold Heraeus RuVac WS 1000 vacuum pump). Pulsed valves (solenoid Parker valve) are used to inject the gas mixture into the reservoir (1 cm³ in volume) where the stagnation pressure is monitored by a pressure transducer (Omega PX170 series). The nozzle assembly is mounted on a movable yoke manually driven from outside the chamber. The nozzles used in this study have been characterized in detail.²¹

C₂H radicals are created coaxially within the uniform supersonic expansion by pulsed laser photolysis of acetylene (C₂H₂) using an unfocused beam at 193 nm (Lambda Physik COMPex Pro 110 ArF). The diameter of the laser beam is limited by the throat of the Laval nozzle (1 cm in diameter). The laser energy is typically ~15 mJ/cm² after the divergent section of the nozzle. The concentration of C₂H radicals inside the flow is monitored by the chemiluminescence tracer method (C₂H + O₂ → CH (A²Δ) + CO₂). The detection zone is situated ~10 cm downstream from the exit of the nozzle where light emitted perpendicular to the molecular beam propagation direction is filtered with a 430±10 nm band-pass filter and detected using a photomultiplier tube. The chemiluminescence signal is recorded using a multichannel scaler (model SR430) in a single photon-counting mode. A typical decay transient is obtained by accumulating ~12,000 photolysis laser pulses. The apparatus is run at a 10 Hz repetition rate. Synchronization of the various experimental components is achieved using a SRS DG535 Digital Delay Generator.

The N₂, O₂ and C₂H₂ gas flows are supplied directly from cylinders through stainless steel lines and controlled by individual calibrated mass flow controllers (MKS Mass-Flo Analog). The 1-butene cylinder is kept in a cold bath at 278 K to lower its vapor pressure, thus preventing condensation in the gas lines. The gases used in these measurements are as follows: the main carrier gas is N₂ (99.999%), C₂H₂ (99.6%) is used as the radical precursor, O₂ (99.998%), 1-butene (98% Sigma Aldrich). The acetylene tank is equipped with an activated charcoal cartridge

1
2
3 filter to remove acetone, present in the tank as a stabilizing agent, prior to mixing in the main gas
4
5 flow.
6
7

8 **2.2. Photoionization Mass Spectrometry (PIMS)**

9
10 The reaction products formed from the reaction of C₂H with 1-butyne are measured in a slow
11 flow tube reactor coupled to tunable vacuum ultraviolet (VUV) synchrotron radiation at the
12 Advanced Light Source in Berkeley.⁵⁰ The Multiplexed Photoionization Mass Spectrometer
13 building upon the general PIMS design of Slagle and Gutman,⁵¹ has been described in previous
14 studies^{17,50,52} and only a brief overview will be given here. The instrument has benefitted from a
15 recent major upgrade: the magnetic sector mass spectrometer described previously has been
16 replaced by an orthogonal accelerated time-of-flight (OA-TOF) mass spectrometer with a
17 superior mass resolution of ~2000. Briefly, the main He gas flow is seeded with the reactants: the
18 C₂H precursor and 1-butyne. All flows are controlled using calibrated mass flow controllers. The
19 pressure inside the flow tube is maintained at 4 Torr (533.3 Pa) by adjusting the pumping speed
20 of the Roots blower using a butterfly valve. At this pressure and room temperature, the total
21 density inside the flow reactor is $1.3 \times 10^{17} \text{ cm}^{-3}$. The densities of the C₂H precursor and 1-butyne
22 are $2.6 \times 10^{16} \text{ cm}^{-3}$ and $5.0 \times 10^{14} \text{ cm}^{-3}$ respectively. The same excimer laser (Lambda Physik
23 COMPex Pro 110 ArF) is used for photolysis but at a lower repetition rate (4 Hz). The measured
24 energy per pulse at the exit of the tube is typically ~27 mJ/cm². The unfocused 193 nm laser
25 beam propagates collinearly down the reactor, a 62 cm long quartz tube with a 1.05 cm inner
26 diameter, generating an initial uniform concentration of C₂H radicals along the tube. The flow
27 velocity inside the reactor is kept constant ~4 m/s. These conditions ensure the photolysis of a
28 fresh gas mixture for each laser pulse. Neutral species escape from a 650 μm diameter pinhole on
29 the side of the quartz tube forming an effusive beam that is skimmed by a 0.15 cm diameter
30 skimmer and crossed by tunable VUV synchrotron radiation (8.1-10.1 eV). All ions are
31 monitored simultaneously using an orthogonal accelerated time-of-flight mass spectrometer
32 equipped with a micro-channel plate detector. Time-dependent, multiplexed mass spectra are
33 recorded as a function of the synchrotron photon energy to obtain Photoionization Efficiency
34 curves (PIE). Different structural isomers of the same chemical formula generally have PIE
35 curves that exhibit unique ionization thresholds (ionization energies), shapes (determined by the
36
37
38
39
40
41
42
43
44
45
46
47
48
49
50
51
52
53
54
55
56
57
58
59
60

1
2
3 Franck-Condon overlap between neutral and cation) and absolute intensities (determined by the
4 electronic transition dipole moment).
5
6

7
8 For the product detection study, the data were taken using 3,3,3-trifluoropropyne ($\text{CF}_3\text{C}_2\text{H}$) as the
9 radical precursor source rather than acetylene (C_2H_2) as was used in the Laval nozzle
10 measurements. This choice was made in order to optimize the signal-to-noise ratio of the two
11 product channels in the mass spectrometer for the title reaction. Indeed, previous experiments¹⁷
12 have shown that $\text{CF}_3\text{C}_2\text{H}$ is a factor of two more efficient than acetylene in producing C_2H
13 radicals at 193 nm. To ensure a linear response of the ion detector, the average ion count rates are
14 limited to 25 kHz. The photolysis of 1-butyne at 193 nm produces photoproducts (mainly
15 propargyl radicals, C_3H_3 , with an IE of 8.67 eV⁵³ and methyl radicals, CH_3) that are additional
16 species that contribute to the total number of ions arriving on the detector. This unwanted
17 photolysis requires using a minimal amount of 193 nm laser fluence in the flow tube. Therefore
18 to avoid detector saturation and to enhance the product ion signals, $\text{CF}_3\text{C}_2\text{H}$ was used as the
19 radical precursor source. Also, above 10.1 eV, the excess reactant, 1-butyne (with an IE of 10.20
20 eV),⁵⁴ in the flow will ionize, increasing the total ion count rate above the acceptable range. With
21 the present experimental apparatus, data could not be obtained above the ionization energy of 1-
22 butyne.
23
24
25
26
27
28
29
30
31
32
33
34
35
36

37 The purities of the different gasses are as follows: He, 99.9999%; $\text{CF}_3\text{C}_2\text{H}$, 99%; C_2H_2 , 99.6%
38 and 1-butyne, 98%. Acetone is removed from the acetylene using a charcoal filter as described in
39 the previous section.
40
41
42
43

44 **2.3. Computational methods**

45
46 Adiabatic ionization energies were calculated using the CBS-QB3 composite method of
47 Petersson and coworkers.^{46,47} Simulated photoionization efficiency curves, based on the
48 geometries, frequencies, and normal coordinates from the CBS-QB3 calculations, were computed
49 using the PESCAL program of Ervin,^{48,49} including full Duschinsky rotation for all totally
50 symmetric modes. The resulting PIE spectra were convolved with a 30 meV FWHM Gaussian
51 function to account for the instrumental resolution. Only the ground electronic states of the
52 cations were included in the calculations, and no attempt was made to predict or model
53
54
55
56
57
58
59
60

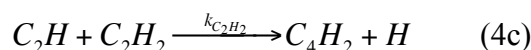
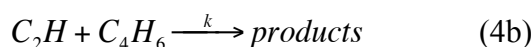
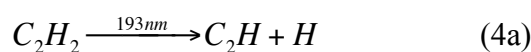
1
2
3 autoionizing resonances. The calculated ionization energies for the C₆H₆ isomers reported in
4 Table 1 are generally within 0.1 eV of the reported experimental values. Our calculated values for
5 the C₅H₄ isomers listed in Table 2 are also in good agreement with reported literature values.
6
7
8
9

10 11 12 **3. Results**

13
14 In this section, the low temperature kinetic measurements will be presented first, followed by the
15 identification of the product channels, identification of the individual isomers and product
16 branching ratios for the reaction in the slow flow tube reactor coupled to VUV synchrotron
17 radiation detection.
18
19
20

21 22 **3.1. Low temperature rate coefficients**

23
24 Since the measured percentage depletion for acetylene, as detailed in Section 3.2.1 below, by the
25 photolysis laser at 193 nm (see Eq. 4a) is only 0.5 %, it can be assumed that the concentration of
26 the ethynyl radicals, [C₂H], is much lower than the concentrations of the molecular species, i.e.
27 1-butyne, acetylene and oxygen. Therefore, C₂H radicals are likely to be consumed in the radical-
28 molecule reactions as shown in Eqs. 4b to 4d rather than radical-radical reactions. A constant
29 amount of O₂ is added in the flow in order to monitor the decay of the C₂H radical concentration
30 as explained below.
31
32
33
34
35
36
37



42
43
44
45
46
47
48 From the reaction scheme outlined above the rate of change of the concentration of C₂H radicals
49 can be expressed as,
50
51
52

$$53 \quad -\frac{d[C_2H]}{dt} = [C_2H](k_{C_2H_2}[C_2H_2] + k_{O_2}[O_2] + k[C_4H_6]) \quad (5a)$$

$$54 \quad = k_{obs}[C_2H]$$

Integrating Eq. 5a with respect to time yields Eq. 5b:

$$[C_2H] = [C_2H]_0 \exp[-k_{obs}t] \quad (5b)$$

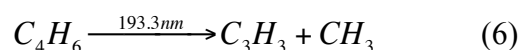
where $k_{C_2H_2}$ and k_{O_2} are the rate constants for the reaction of the ethynyl radical with acetylene and oxygen respectively. $[C_2H]_0$ is the initial concentration of ethynyl radicals. The rate constant for the reaction of C_2H with 1-butyne, k , is determined by plotting the pseudo first-order rate constants, k_{obs} , as a function of the concentration of 1-butyne, $[C_4H_6]$, while keeping the concentrations of oxygen and acetylene constant. Chemiluminescence from the electronically excited CH ($A^2\Delta$) state (see Eq. 4d) at 431.22 nm⁵⁵ is used to monitor the time evolution of the C_2H radicals in the Laval flow. Because the radiative lifetime for free CH ($A^2\Delta$) radicals (440(\pm 20) ns)⁵⁶ is much shorter than the reaction timescale of the ethynyl radicals, a quasi-steady-state approximation can be made for the concentration of CH ($A^2\Delta$). Therefore, it can be assumed that the chemiluminescence emission is directly proportional to the concentration of C_2H radicals present in the collimated supersonic expansion.

Figure 1 shows a typical decay trace of the chemiluminescence signal as a function of time. The experimental data can be fit by a single exponential function and confirms the pseudo-first-order approximation made in Eqs. 5a and 5b. The time interval for the fit for each decay curve is $15 < t < 200 \mu s$, hence avoiding interference from scattered light and emission produced by the 193 nm laser pulse. This initial 15 μs time delay also allows for the quenching of excited C_2H radicals by nitrogen molecules.⁵⁷ As reported previously in the study of the reaction of C_2H with benzene,¹⁶ the typical quenching time of excited ethynyl radicals in the flow is less than 1 μs .

The kinetic measurements are repeated for different concentrations of 1-butyne while keeping the concentrations of acetylene and oxygen constant. As shown in Figure 2, the plot of k_{obs} as a function of the concentration of 1-butyne is fit well by a straight line, whose slope is the rate constant, k , for the $C_2H + 1$ -butyne reaction. This procedure is repeated using different Laval nozzles to examine the temperature dependence of the rate coefficient. At each temperature, k_{obs} is typically measured for nine to twelve different 1-butyne densities. The error bars for k_{obs} are

1
2
3 determined to be $\pm 2\sigma$ of the single exponential fits. The accumulated uncertainties for the
4 concentrations of 1-butyne (i.e. 0.5% depletion by the 193 nm laser and 1% error of the actual
5 flow controller) are not shown in Figure 2. The values of the rate coefficients as a function of
6 temperature are summarized in Table 3. The reported uncertainties for these measurements are
7 20 % and are discussed below.
8
9
10
11

12
13
14 At 193 nm and room temperature, the reported absorption cross-section for 1-butyne is
15 significant ($\sim 1 \times 10^{-18} \text{ cm}^2$).⁵⁸ As will be discussed in Section 3.2.1, our measurements indicate
16 that the depletion in 1-butyne and acetylene are comparable, i.e. ~ 0.5 %. Therefore, we can
17 assume that the destruction of 1-butyne at 193 nm is negligible and does not affect the reported
18 densities in the flow. No chemiluminescence signal at ~ 430 nm is detected in the absence of the
19 C_2H precursor, indicating that the C_2H photodissociation channel of 1-butyne is not significant.
20 We identified C_3H_3 and CH_3 as the main photodissociation products of 1-butyne (see Eq. 6 and
21 Section 3.2.1). So we conclude that acetylene photodissociation is the only source of C_2H radicals
22 and that the single photon photodissociation of 1-butyne does not produce C_2H radicals in
23 significant amounts so as to interfere with the reaction. Again, based on the percentage depletion
24 measurements (radical species) and the actual densities of the reagents (molecular species) in the
25 flow, the probability of radical-radical removal of C_2H is negligible compared to removal by
26 radical + stable molecule reactions.
27
28
29
30
31
32
33
34
35
36
37



38
39
40
41
42 Decreasing the energy of the photolysis laser by a factor of 2 did not change the measured rate
43 constants significantly. Fitting the present data to a temperature-dependent rate expression yields
44 $k = (2.4 \pm 0.5) \times 10^{-10} (\text{T}/295 \text{ K})^{-(0.04 \pm 0.03)} \text{ cm}^3 \text{ molecule}^{-1} \text{ s}^{-1}$. However, as the temperature
45 dependence is essentially negligible within the experimental uncertainties, we recommend for
46 kinetic modeling that the average rate coefficient, $k = 2.5 \times 10^{-10} \text{ cm}^3 \text{ molecule}^{-1} \text{ s}^{-1}$, should be
47 taken with a total uncertainty of 20%.
48
49
50
51
52
53
54
55
56
57
58
59
60

3.2. Tunable VUV isomer-specific product detection

The goal of product detection studies coupled with kinetics measurements is to identify and estimate branching ratios for the products of the reaction between the ethynyl radical with 1-butyne. In this respect, the reaction has been studied at 295 K and 533 Pa in the slow flow reactor using Multiplexed Photoionization Mass Spectrometry (MPIMS) with tunable VUV synchrotron radiation. Both time- and energy-resolved data have been collected as described in Section 2.2. Mass spectra as a function of the ionization energy are retrieved from the raw data by integrating over the whole reaction timescale of 80 ms. Note that mass spectra are also taken for 20 ms before the pulsing of the photolysis laser for background subtraction. In this way, identification by m/z ratio of all species involved in the reaction is obtained. Then, for a given mass, the evolution of the ion signal as a function of: (1) time, which reveals the chemical nature of the species, i.e. precursor, photolysis product, primary reaction product, or secondary reaction product, and (2) energy, which helps to determine and distinguish between different isomers, is analyzed. Indeed, the presence of different isomers with different ionization energies is revealed as different thresholds and shapes in the Photoionization Efficiency (PIE) curves.

Figure 3(a) shows a mass spectrum with the radical precursor and the reactant, 1-butyne, flowing in the buffer gas and Figure 3(b) shows a second mass spectrum with only 1-butyne, both acquired at 10.1 eV and integrated over 80 ms of reaction time, with the 193 nm photolysis laser and the same density of 1-butyne. Both mass spectra are background subtracted. Two mass peaks show a significant increase when the C_2H precursor is added: $m/z = 64$ and $m/z = 78$. Given the measured rate coefficient for the reaction of C_2H with 1-butyne, the concentration of the reactants and the instrumental time resolution, it is not possible to measure the rise-time of these two products. However, the observed instrument-limited rise-time after the photolysis laser pulse and the fact that the ion signal for both masses remains constant at later times is consistent with the formation of a closed-shell, unreactive species. After careful inspection of the mass spectra in Figure 3, the following observations can be made:

1. The ion signal at $m/z = 64$ (C_5H_4) is almost entirely due to the simultaneous presence of C_2H , created by the photolysis laser, and 1-butyne. This result is consistent with the $C_5H_4 + CH_3$ product channel for the title reaction.

- 1
2
3 2. The ion signal at $m/z = 78$ (C_6H_6) shows a significant enhancement (by a factor of ~ 6)
4 when the radical precursor is added to the flow. This result is consistent with the $C_6H_6 +$
5 H product channel for the title reaction. But, it is noted that there is some background
6 contribution to the $m/z = 78$ ion signal in the absence of the C_2H radical precursor.
7
8
9

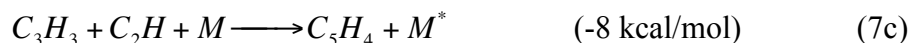
10
11 Before analyzing these two ion signals, it is important to identify any side reactions that might
12 interfere with the two product channels (see Section 3.2.1). As mentioned in Section 3.1, 1-
13 butyne has a significant photodissociation cross-section at 193 nm, giving rise to additional
14 radical species that can react with the reagents in the flow. In order to evaluate the contribution of
15 these photodissociation products and extract the true signals for the title reaction, two separate
16 sets of data, with the same concentration of 1-butyne in the flow, were collected (with and
17 without the radical precursor). As seen in Figure 3(b), the contribution of 1-butyne
18 photodissociation products to $m/z = 64$ ion signal is negligible, showing that C_5H_4 is indeed the
19 product of the CH_3 -loss channel for the title reaction. The PIE curve is analyzed in Section 3.2.2.
20 However, the side reactions that produce $m/z = 78$ ion signal are not negligible. Therefore, we
21 extracted from the two sets of data a PIE curve for $m/z = 78$ ions with (\blacklozenge) and without (\otimes) the
22 radical precursor (see Figure 4 and caption for details). In this way, the increase in the ion signal,
23 i.e. (\blacklozenge) minus (\otimes), is the contribution of products from the title reaction products to the $m/z = 78$
24 ion signal. The result is a PIE curve for the C_6H_6 product channel, which is analyzed in Section
25 3.2.3. Estimates of branching ratios are also derived for each product channel. Note that complete
26 data sets in our experiment are limited to VUV photon energies between 8.2 and 10.1 eV due to
27 experimental limitations as detailed in Section 2.2.
28
29
30
31
32
33
34
35
36
37
38
39
40
41
42

43 **3.2.1. Photodissociation and photoproducts of reactants at 193 nm**

44
45
46 Figure 5 shows the photo-depletion measurements of (a) 1-butyne, (b) acetylene and (c) 3,3,3-
47 trifluoropropyne recorded at 193 nm. These experiments have been done in order to quantify the
48 photo-depletion of 1-butyne by the laser and to choose between acetylene and 3,3,3-
49 trifluoropropyne for the C_2H precursor. Each data set is fit to a step function after the pulsing of
50 the laser at 20 ms. The average laser energy is ~ 27 mJ/pulse in all experiments and the measured
51 percentage depletion as well as the composition of the gas mixtures are reported in Table 4. From
52 these measurements, it can be noted that the photodepletion of 1-butyne and acetylene are
53
54
55
56
57
58
59
60

comparable, i.e. 0.45% and 0.47% respectively. As expected,⁵⁹ the photodissociation of 3,3,3-trifluoropropyne is more efficient by a factor of 2 (0.83%) compared to acetylene. In addition to the high yield of C₂H radicals, the photolysis of CF₃C₂H leaves behind less reactive CF₃ radicals compared to H-atoms from acetylene. We have used 3,3,3-trifluoropropyne as the C₂H radical precursor in order to optimize the signal for the two product channels because it allows us to increase the concentration of ethynyl radicals while keeping the 193 nm laser energy low enough to minimize 1-butyne photodissociation.

As mentioned in the previous section, 1-butyne has a significant photodissociation cross-section at 193 nm. It is most likely that the photoproducts are radical species that can further react with 1-butyne to yield stable hydrocarbons. These products can interfere with the product channels of the title reaction. Quantifying the contribution of these photodissociation products of the alkyne to the ion signals is therefore crucial in our experiment for accurate isomer-specific product detection. We have identified methyl (CH₃, IE = 9.843 eV)⁶⁰ and propargyl (C₃H₃, IE = 8.67 eV)⁵³ as the two main radical species formed from the 193 nm photolysis of 1-butyne (not shown on mass spectra of Figure 3). CH₃ radicals can react with C₄H₆ or CF₃C₂H molecules in the flow. However, it is unlikely that the products of the reaction will contribute to the ion signal at either m/z = 64 (C₅H₄) or 78 (C₆H₆). On the other hand, C₃H₃ radicals could react with C₄H₆ to produce C₆H₆ (e.g. benzene) by losing a CH₃ radical according to Eq. 7a. The formation of C₅H₄ (e.g. methylidyne) is found to be endothermic (Eq. 7b) and therefore not favorable. C₃H₃ radicals could also react with CF₃C₂H to produce C₅H₄ by losing a CF₃ radical.



However, reactions of propargyl with closed-shell molecules are relatively slow. On the other hand, recombination of two propargyl radicals could be a source of C₆H₆ (Eq. 1). Similarly, C₃H₃ + C₂H could be a source of C₅H₄ as shown in Eq. 7c, and it is unlikely that C₂H + C₂H will contribute to the ion signal at either m/z = 64 (C₅H₄) or 78 (C₆H₆). At the pressure of the present experiments (533 Pa), it is expected that stabilization dominates the propargyl + propargyl

1
2
3 reaction, with only about 10^{-3} branching to phenyl + H.⁶¹ Based on these considerations, we
4 identify $C_3H_3 + C_3H_3$ as the main side reaction contributing to the $m/z = 78$ ion signal for pure 1-
5 butyne photolysis. By flowing only the C_2H precursor in the buffer gas, we verified that no
6 contribution of trifluoropropyne photoproducts to the two mass channels of interest was
7 observed.
8
9

10
11
12
13
14 Figure 4 shows the PIE curves with and without the C_2H precursor for $m/z = 78$ ion signal.
15 Assuming that the main interference in the $m/z = 78$ ion signal is the product of $C_3H_3 + C_3H_3$ (Eq.
16 1) and that C_6H_6 is one product of the $C_2H + 1$ -butyne reaction as shown in Eq. 4b and discussed
17 above, we can subtract the $m/z = 78$ ion signal resulting from propargyl recombination obtained
18 without C_2H radicals present from the total ion signal for $m/z = 78$ when C_2H radicals are
19 present. This process yields the PIE curve for the title reaction, which is shown in Figure 6. For
20 $m/z = 64$ (C_5H_4), the PIE curve is shown in Figure 7. In the sections to follow, these two PIE
21 curves are analyzed and estimates of branching ratios are derived for the C_5H_4 and C_6H_6 product
22 channels.
23
24
25
26
27
28
29

31 **3.2.2. C_5H_4 from the reaction of the ethynyl radical with 1-butyne**

32
33

34 Figure 7 shows the PIE curve for the C_5H_4 mass channel for the reaction of the ethynyl radical
35 with 1-butyne. In our analysis of the observed PIE curve below, literature and calculated values
36 of the ionization energies of the C_5H_4 isomers are taken from the work of Goulay and
37 coworkers¹⁷ and Hansen and coworkers.⁶² Because the absolute photoionization cross sections
38 are not available for all of the C_5H_4 isomers, we have used the single point estimates of
39 photoionization cross sections already reported.¹⁷ Hansen and coworkers⁶² performed Franck-
40 Condon simulations for ethynylallene ($CH_2CCHCCH$), methylidyneacetylene and 1,4-pentadiyne in
41 their study of C_5H_x isomers⁶² for an assumed temperature of 300 K. The simulated
42 photoionization efficiency curves are in very good agreement with their experimental data for the
43 C_5H_4 isomers. In the absence of any reference data for these isomers, these simulated curves are
44 used to fit our experimental data.
45
46
47
48
49
50
51
52
53

54
55 The observed PIE curve shown in Figure 7 can be fit between 8.1 and 9.9 eV by a weighted sum
56 of Franck-Condon based simulations for the two most stable isomers of C_5H_4 , i.e. ethynylallene
57
58
59
60

1
2
3 and methyldiacetylene. Since no threshold in the ion signal is observed at 8.67 eV, we conclude
4 that the 1,2,3,4-pentatetraene isomer is not produced by the reaction. The first sharp rise in the
5 ion signal at 9.15 eV is attributed to the presence of ethynylallene. The only reported adiabatic
6 ionization energy for this isomer is 9.22 eV using QCISD(T) calculations,⁶² in good agreement
7 with our calculated value of 9.20 eV. The solid black line in Figure 7(a) indicates the fit including
8 only the contribution of the CH₂CCHCCH isomer. Note that the calculated photoionization
9 efficiency curve increases slowly above 9.25 eV with a step around 9.5 eV,⁶² almost coinciding
10 with the next threshold in the ion signal. However, the fit assuming only ethynylallene
11 contributes to the PIE curve between 8.1 and 9.9 eV is fairly poor, which suggests the presence of
12 an additional isomer. It follows that the threshold at 9.5 eV is most certainly due to the presence
13 of methyldiacetylene. Moreover, there is a good agreement between the simulated PIE curve and
14 the actual experimental data, as seen in Figure 7(b), when the contribution from
15 methyldiacetylene is taken into account in the overall fit up to 9.9 eV.
16
17
18
19
20
21
22
23
24
25
26
27

28 The observed signal as a function of energy, $S(E)$, is proportional to the sum of the individual
29 photoionization cross sections, $\sigma_i(E)$, weighted by the mole fraction of each C₅H₄ isomer, X_i , as
30 indicated in Eq. 8. Reliable estimates for the photoionization cross sections can be obtained as
31 described¹⁷ using a semi-empirical model by Bobeldijk and coworkers.⁶³ With the reported
32 values,¹⁷ we can estimate a ratio for ethynylallene/methyldiacetylene of approximately 4:1 for the
33 reaction of the ethynyl radical with 1-butyne.
34
35
36
37
38
39
40

$$41 \quad S(E) \propto \sigma_{total}(E) = \sum_{i=1}^m \sigma_i(E) X_i \quad (8)$$

42
43
44
45

46 Due to experimental limitations as described in Section 2.2, a complete set of data above
47 10.125 eV could not be obtained. Therefore, in our experiment we cannot probe the presence or
48 absence of 1,4-pentadiyne (IE = 10.27 eV).⁵⁴ The gray dashed line in Figure 7(b) represents the
49 calculated PIE curve of 1,4-pentadiyne. The residual of the fit with ethynylallene and
50 methyldiacetylene in Figure 7 suggests the presence of another ionization threshold near 9.95 eV.
51 However, as seen by Goulay and coworkers¹⁷ in the reaction of C₂H + propyne, the ion signal for
52 m/z = 64 should follow a slight linear increase as a function of photon energy above 9.8 eV when
53
54
55
56
57
58
59
60

1
2
3 only ethynylallene and methyldiacetylene are present. This would suggest that the observed
4 threshold in our experiment might be due to the presence of another C_5H_4 isomer. Nevertheless,
5 based on the molecular structure of methyldiacetylene (IE = 9.47 eV) and 1,4-pentadiyne (IE =
6 10.27 eV), i.e. both molecules have two triple bonds, compared with ethynylallene (with a lower
7 IE = 9.20 eV), which has two double bonds and a single triple bond, it is hard to propose a
8 rational structure of a linear C_5H_4 isomer that could possibly have an ionization energy around 10
9 eV. Also, this threshold feature could be explained by dissociative ionization of a heavier
10 molecule or the presence of an electronically excited state of $C_5H_4^+$. Again, in the absence of a
11 complete set of data at higher photon energies, we can only quantify the isomeric distribution of
12 methyldiacetylene and ethynylallene.
13
14
15
16
17
18
19
20
21
22

23 The fit of the PIE curve, indicated as a thick black line is shown in Figure 7(b), is the sum of the
24 individual contributions (FC simulations) of ethynylallene (dashed line) and methyldiacetylene
25 (dotted line). The PIE curve is normalized to the total estimated cross section at 9.8 eV of an
26 average mixture of 82(\pm 15)% of ethynylallene and 18(\pm 15)% of methyldiacetylene using
27 estimated photoionization cross sections reported in Table 5.
28
29
30
31

32 **3.2.3. C_6H_6 from the reaction of the ethynyl radical with 1-butyne**

33
34
35

36 Figure 6 shows the photoionization efficiency curve for $m/z = 78$ (C_6H_6) mass channel, from the
37 reaction of the C_2H radical and 1-butyne. Relative photoionization efficiency curves are used
38 when available for some of the C_6H_6 isomers considered herein.⁶⁴ The 8.2-9.1 eV range exhibits a
39 very slow monotonic rise in the ion signal. At 8.36 eV a first threshold is observed,
40 corresponding to the ionization energy of the cyclic 5-membered C_6H_6 isomer, fulvene.
41 Furthermore, the onset of the signal can be replicated by its relative PIE curve.⁶⁴ A second
42 threshold is identified at 8.8 eV. In this portion of the PIE curve, a single contribution by fulvene
43 cannot account for the observed signal as shown in Figure 6(b). This second onset corresponds to
44 the ionization energy of 3,4-dimethylenecyclobut-1-ene (DMCB), a 4-membered cyclic isomer of
45 C_6H_6 . A good fit is obtained with a weighted sum including the relative PIE curves for fulvene
46 and DMCB, further confirming the presence of the latter. Using estimated values⁴⁴ for the
47 photoionization absorption cross sections of these two species (see Table 6), these isomers are
48 formed in an approximate ratio of 1:2.
49
50
51
52
53
54
55
56
57
58
59
60

1
2
3
4
5 The residual of the fit including fulvene and DMCB (thick black line in Figure 6(b)) indicates a
6 small feature between 8.9-9.4 eV followed by a sharp increase in the photoionization signal
7 around 9.4 eV. In this energy range, there are four possible C₆H₆ isomers: 2-ethynyl-1,3-
8 butadiene (IE = 8.95 eV), 3,4-hexadiene-1-yne (IE = 8.99 eV), benzene (IE = 9.24 eV)⁶⁵ and 1,3-
9 hexadiyne (IE = 9.41 eV⁶⁶). The relative PIE curve of benzene is well known⁶⁴ while those of 2-
10 ethynyl-1,3-butadiene, 3,4-hexadiene-1-yne and 1,3-hexadiyne have been computed as discussed
11 in Section 2.3. Benzene has a very distinctive onset and characteristic PIE curve⁶⁴ shape that does
12 not seem to match with the feature observed around 9.3 eV. Since the small onset occurs before
13 the well-defined ionization potential of benzene, the small feature is more likely related to 2-
14 ethynyl-1,3-butadiene and 3,4-hexadiene-1-yne. Indeed, a good fit (solid black line) of the
15 experimental data is obtained up to 9.35 eV when a weighted contribution of 2-ethynyl-1,3-
16 butadiene (dotted line) and 3,4-hexadiene-1-yne (dashed line) is included as shown in Figure
17 6(c). Note that the calculated IE of 1,3-hexadiene-5-yne (8.63 eV) is found to be 0.6 eV lower
18 than the reported experimental value (9.3 eV), which is an estimated value from electron impact
19 measurements.⁶⁶ No threshold in the ion signal is observed around 8.6 eV indicating that 1,3-
20 hexadiene-5-yne is not produced in significant amounts. Although it is therefore difficult to
21 firmly quantify benzene in our experiment, it is probably not produced in significant quantities.
22
23
24
25
26
27
28
29
30
31
32
33
34
35
36

37 It is likely that the next threshold observed at 9.4 eV is due to the linear C₆H₆ isomer, 1,3-
38 hexadiyne. Additional thresholds above 9.4 eV are not observed, indicating that 1,4-hexadiyne
39 and 1,5-hexadiyne are also negligible reaction products. The fit of the PIE curve, indicated as a
40 thick black line, is the sum of the individual contributions (FC simulations) of fulvene, DMCB,
41 2-ethynyl-1,3-butadiene, 3,4-hexadiene-1-yne and 1,3-hexadiyne. The PIE curve is normalized to
42 the total estimated cross section of an average mixture of 18% of fulvene, 32% of DMCB, 8% of
43 2-ethynyl-1,3-butadiene, 28% of 3,4-hexadiene-1-yne and 14% of 1,3-hexadiyne using the
44 estimated photoionization cross sections at 10 eV (see Table 6). Within experimental
45 uncertainties, an upper limit of 10 % is estimated for benzene production.
46
47
48
49
50
51
52
53
54
55
56
57
58
59
60

4. Discussion

In this paper, we present the only experimental work reporting both low temperature kinetics and room temperature product detection of the ethynyl radical (C_2H) with a C_4 molecule, 1-butyne. The rate coefficient measurements, within experimental uncertainty, exhibit almost no temperature dependence in the 74-295 K range as shown in Figure 8. Using photoionization mass spectrometry coupled to tunable VUV synchrotron radiation, we have direct information about the product channels involved (4 Torr, 295K) and we have been able to determine and distinguish between the different isomers present. We discuss below the probable mechanism for the reaction of the C_2H radical and 1-butyne and the possible implications for the photochemistry of the outerplanets, especially the Saturnian moon Titan.

4.1. Temperature dependence and reaction mechanism

It is worthwhile to compare the measured rate coefficients of the reaction of the C_2H radical with 1-butyne (or ethylacetylene) with the smaller alkynes, i.e. acetylene (C_2H_2) and propyne (or methylacetylene, C_3H_4). Figure 8 shows a plot of the rate constants for the title reaction as a function of temperature along with analogous measurements for acetylene and propyne obtained in a collaborative work between Leone and coworkers and Sims and coworkers.^{13,25} As pointed out by Sims and coworkers¹³, the results obtained independently using a pulsed and a continuous Laval nozzle are in satisfactory agreement. Moreover, a general rule of thumb is derived by taking the measured rate coefficient for acetylene ($k_{C_2H_2} = 1.9 \times 10^{-10} \text{ cm}^3 \text{ molecule}^{-1} \text{ s}^{-1}$ at $T \approx 50 \text{ K}$) and its ionization energy of 11.4 eV as a reference to estimate low temperature rate coefficients of C_3 and C_4 alkenes and alkynes as a function of their ionization energies. Using this correlation, it is expected that the rate constant should increase with molecular mass (or decreasing ionization energy) for the corresponding alkenes, alkynes, dienes and diynes. As shown in Figure 8, the measured rate coefficient with C_4H_6 ($k = 2.6 \times 10^{-10} \text{ cm}^3 \text{ molecule}^{-1} \text{ s}^{-1}$ at $T \approx 74 \text{ K}$) is higher than C_2H_2 but comparable with C_3H_4 and is therefore in agreement with the expected trend. It should be noted that in the temperature range 70-100 K, the reaction with the C_2H radical is rapid and close to the collision-determined limit. Our data is also consistent with the measured rate coefficients of the C_2H with 1,3-butadiene reaction.³⁹ Indeed, our rate constant is slightly lower

1
2
3 than the C_4 diene ($k_{C_2H} = 2.9 \times 10^{-10} \text{ cm}^3 \text{ molecule}^{-1} \text{ s}^{-1}$ at $T \approx 104 \text{ K}$), which is in agreement with
4
5 the lower ionization energy of 9.072 eV^{67} for 1,3-butadiene. No measurements of rate
6
7 coefficients for the reactions of C_2H and the two other linear C_4H_6 isomers, i.e. 1,2-butadiene (IE
8
9 = 9.03 eV^{68}) and 2-butyne (IE = 9.59 eV^{54}) are available. However, our results combined with
10
11 previous studies³⁹ suggest that the rate coefficients for these reactions should be comparable. The
12
13 reaction of the C_2H radical with linear C_4H_6 isomers is most probably barrierless, showing almost
14
15 no temperature dependence and a rate coefficient can be estimated to be in the range $(2.5\text{-}3.0) \times$
16
17 $10^{-10} \text{ cm}^3 \text{ molecule}^{-1} \text{ s}^{-1}$.

18
19
20 Before considering the possible mechanism for the reaction, it is useful to compare the energetics
21
22 of propargyl recombination,⁶¹ which has been identified as a benzene formation pathway in fuel-
23
24 rich flames.⁴⁴ Figure 9 shows the heats of reaction (ΔH_r° in kcal/mol) in which the three most
25
26 stable C_6H_6 isomers, i.e. DMCB, fulvene and benzene, are produced. The three-body
27
28 recombination of two propargyl radicals leading to C_6H_6 isomers is more exothermic (~ 38
29
30 kcal/mol) compared to the formation of the same isomers through the H-loss channel of $C_2H + 1$ -
31
32 butyne reaction. In the latter case, the C_6H_6 products are left with less internal energy and as a
33
34 consequence further isomerizations on the C_6H_6 potential energy surface to form more stable
35
36 isomeric structures, e.g. DMCB to fulvene or fulvene to benzene, are probably less facile. In fact,
37
38 most of the isomerization transition states calculated by Miller and Klippenstein are predicted to
39
40 be energetically inaccessible for the C_6H_6 product of the $C_2H + 1$ -butyne reaction, so the
41
42 isomerization steps that determine the product distribution most likely take place on the C_6H_7
43
44 surface. The heats of formation of methyldiacetylene (-39 kcal/mol), diacetylene (-36 kcal/mol)
45
46 and DMCB (-43 kcal/mol) for the title reaction are all comparable. Because methyldiacetylene
47
48 and DMCB are detected in the reaction at room temperature, the C_2H_5 -loss channel to form C_4H_2
49
50 (diacetylene) is presumably also accessible. However, the ionization energy of diacetylene, 10.17
51
52 eV, is too close to that of 1-butyne, and we cannot operate at high enough photon energies to
53
54 directly probe this channel in our experiment.

55
56 Reactions of non-resonance-stabilized carbon-centered radicals with unsaturated hydrocarbons
57
58 are expected to proceed *via* an intermediate^{16,17,69} formed with almost no activation energy.⁴⁵
59
60 Subsequently, the short-lived intermediate decomposes to give the final products of the reaction

1
2
3 whose isomeric structure depends upon the energy available in the system. Within the
4 temperature range 74-295 K and pressure range 0.1-1 Torr, the measured total rate coefficient for
5 the reaction is almost constant, and close to the collision-determined limit as mentioned above.
6 This behavior suggests that back dissociation of the intermediate is negligible. Also for the
7 reaction between C_2H and acetylene, as shown experimentally^{15,21,22} and theoretically,^{15,70} the
8 entrance channel of the reaction is the attack of the π electrons by the radical to form an
9 intermediate that in turn decomposes to give diacetylene as the final product, consistent with an
10 addition-elimination reaction. The hydrogen abstraction mechanism whereby a H-atom is
11 captured by the C_2H radical to form acetylene is also thermodynamically feasible. In the case of
12 $C_2H + C_2H_2$, Ceursters and coworkers¹⁵ calculated a barrier of ~ 40 - 45 kJmol^{-1} for the direct H-
13 abstraction while addition-elimination of C_2H is essentially barrierless. The close to collision-
14 determined limit rates of reaction indicate that addition-elimination predominates over
15 abstraction in such reactions involving the C_2H radical with hydrocarbons.¹⁷
16
17
18
19
20
21
22
23
24
25
26
27

28 By analogy to the study of Ceursters and coworkers,¹⁵ it is expected that the C_2H radical will add
29 to the triple bond of the 1-butyne molecule. In principle, the C_2H addition proceeds by the direct
30 attack on either of the triply bonded carbon atoms, giving rise to an acyclic radical species.¹⁵ In
31 the reaction of C_2H with acetylene, the cyclic three-membered and four-membered ring radicals
32 are found to be far less stable compared to the open radical structure. Moreover, the three-
33 membered ring radical can easily rearrange to the open form because both structures are
34 separated by a barrier of 5.7 kcal/mol (24 kJ/mol).¹⁵ A similar situation can be expected for the
35 title reaction. The initially formed radical can isomerize prior to dissociation. Senosiain and
36 Miller⁷¹ have reported several stationary points of C_6H_7 related to the addition of acetylene to *n*-
37 and *i*- C_4H_5 radicals. The intermediates in those reactions are not directly relevant to the present
38 reaction, but because the $C_2H + 1$ -butyne asymptote lies higher in energy than many of the
39 calculated isomerization transition states, that work is consistent with relatively facile
40 isomerization of the initially formed C_6H_7 adduct in the $C_2H + 1$ -butyne reaction.
41
42
43
44
45
46
47
48
49
50
51
52

53 Starting with the radical formed by the direct attack of the terminal acetylenic carbon atom by
54 C_2H (see Figure 10), four different pathways leading to stable products (C_3H_4 and C_6H_6 isomers)
55 can be proposed. These pathways include three different direct β scission reactions to
56
57
58
59
60

1
2
3 ethynylallene formation *via* CH₃-loss or either 1,3-hexadiyne or 3,4-hexadien-1-yne *via* H-loss. A
4
5 1,3 H shift followed by a H-loss, through a β scission, could form another linear C₆H₆ isomer,
6
7 1,3-hexadien-5-yne. The barrier to a 1,3 H shift should be substantial,⁷² but may still lie beneath
8
9 the reactant energy.

10
11
12 Similarly, three different evolution pathways can be proposed in the case of C₂H addition to the
13
14 central carbon atom in the triple bond (see Figure 11). First, direct C₂H₅-loss through a β scission
15
16 reaction can lead to diacetylene (C₄H₂). Second, a 1,4 H shift followed by β scission forms 2-
17
18 ethynyl-1,3-butadiene or cyclization to a five-membered ring radical, which eventually
19
20 decomposes to yield fulvene. Third, a 1,3 H shift followed by cyclization to form the four-
21
22 membered radical structure can ultimately decompose to give 3,4-dimethylenecyclobut-1-ene
23
24 through β scission.

25
26
27 Based on the proposed reaction pathways, the formation of C₅H₄ isomers most probably results
28
29 from terminal addition of the C₂H radical to 1-butyne (see Figure 10). As seen from the PIE
30
31 curve in Figure 7, the 4:1 ratio in favor of the ethynylallene suggests that the diene is formed
32
33 preferentially as opposed to methyldiacetylene in the reaction between C₂H with 1-butyne. This
34
35 observation is consistent with the proposed mechanism where ethynylallene production is facile,
36
37 because it results from a direct CH₃-loss through a β scission reaction of the adduct formed after
38
39 terminal addition. Ultimately, the branching ratio for isomerization to methyldiacetylene will
40
41 probably depend on the amount of internal energy left in ethynylallene after reaction. Moreover,
42
43 the geometries of the adducts shown in Figures Figure 10 and Figure 11 suggest that 1,4-
44
45 pentadiyne formation is more complex than formation of ethynylallene. It can be argued that the
46
47 rearrangement leading to its formation is probably unfavorable.

48
49 As suggested by the branching ratios of 18(±5)% and 32(±8)% for fulvene and 3,4-
50
51 dimethylenecyclo-but-1-ene (DMCB) respectively, 4- and 5-membered ring species are produced
52
53 in comparable proportions to the linear C₆H₆ isomers, i.e. 8(±5)% of 2-ethynyl-1,3-butadiene,
54
55 28(±8)% of 3,4-hexadiene-1-yne and 14(±5)% of 1,3-hexadiyne. At the present time, there is no
56
57 potential energy surface available for the reaction between the C₂H radical and C₄H₆. However,
58
59 the related systems of *n*- and *i*-C₄H₅ + acetylene⁷¹ and the recombination of two propargyl
60

radicals on a C_6H_6 potential energy surface⁶¹ provides some insight into possible isomerization pathways. The benzene molecule has the deepest well, on the C_6H_6 surface, followed by fulvene and DMCB. Our measurements demonstrate that benzene is probably not formed in significant amounts by this reaction at room temperature, where an upper limit of 10 % is estimated. The isomerization of DMCB or fulvene down to benzene must traverse substantial barriers. For instance, in the calculated fulvene to benzene paths,⁶¹ benzene is the lower of the two isomers by about 31 kcal/mol (130 kJ/mol). However, approximately 75 kcal/mol (~314 kJ/mol) is required to overcome the barrier to isomerization. The presence of fulvene and DMCB products demonstrates that cyclization occurs in the $C_6H_6 + H$ channel but suggests that the energy remaining in the C_6H_6 product is not enough to readily overcome the barrier to benzene formation. However, the isomerization on the C_6H_7 surface may be more facile. Calculated transition states for the 1,5- and 1,3-H shifts from other C_6H_7 isomers produced in the $C_4H_5 +$ acetylene reactions⁷¹ lie near or below the energy of the $C_2H + 1$ -butyne reactants. It seems likely that the isomeric product distributions are largely determined by the dynamics on the C_6H_7 surface. Although the total rate coefficient is found to be independent of temperature over the range studied, the product distributions could still be temperature dependent.

4.2. Implication for Titan's photochemistry

Reactions of unsaturated C_2 hydrocarbon radicals⁷³ with hydrocarbon species are considered to play a central role for the formation of carbon rich species (polyynes and PAHs) in the interstellar medium, exo-planets and in the cold, photochemically active atmosphere on Titan.^{6,74} In the course of these reactions, eventually two more carbon atoms are incorporated, thereby enlarging the carbon chain in the molecule and contributing to the complex process of molecular weight growth. These reactions can proceed *via* multiple intermediates, leading to different product channels and the initial isomeric structure can play a crucial role as demonstrated in the study with C_3H_4 isomers.¹⁷ Moreover, this study of 1-butyne shows that at least two competing product channels (H-loss and CH_3 -loss) are active and of almost equal importance. In the case of acetylene, the mechanism involves the initial addition of the C_2H group to the π -electron system followed by the elimination of a hydrogen atom to form the product, diacetylene (C_4H_2). The measured rate constant is near the collision limit and increases as a function of the number of carbon atoms in the chain. In devising ever more elaborate models for Titan's atmosphere, low

1
2
3 temperature rate coefficient data including C_4 and longer chain hydrocarbons will be required. In
4 this respect, the low temperature kinetic measurements for the title reaction, together with the
5 previous study of 1,3-butadiene³⁹ in our group, indicate that the reactions with C_4H_6 isomers can
6 occur at rates close to the collision limit at temperatures relevant to Titan's atmosphere, i.e. on
7 the order of $(2.5-3.0) \times 10^{-10} \text{ cm}^3 \text{ molecule}^{-1} \text{ s}^{-1}$.
8
9

10
11
12
13
14 In this work, we also estimated the product branching ratios for the reaction of the C_2H radical
15 with 1-butyne at room temperature and 4 Torr (533 Pa). Special care needs to be taken because it
16 is known that extrapolation of data to lower temperatures is often problematic. However, the low
17 temperature kinetic measurements for the reaction of the ethynyl radical with 1-butyne do not
18 show any temperature dependence in the range 74-295 K. This behavior is indicative of a
19 reaction without an activation barrier. In this case, the rate-limiting step of the reaction is the
20 addition of the C_2H radical to the triple bond and the entrance channel of the reaction can be
21 expected to be the same down to low temperatures as discussed by Goulay and coworkers.¹⁷ It is
22 therefore probable that reactions of the C_2H radical with C_4H_6 molecules can contribute to
23 molecular weight growth through the addition and subsequent elimination of a H-atom or methyl
24 radical giving rise to C_5 and C_6 carbonaceous species. Diacetylene could also be a favorable exit
25 channel.
26
27
28
29
30
31
32
33
34
35
36

37 The distribution of C_6H_6 isomers might be significantly altered at low temperatures. For instance,
38 if thermal energy is required for isomerization of the initial adduct that leads to the formation of
39 small 4- and 5-membered cyclic molecules, then this pathway could be disfavored at lower
40 temperatures. However, the exothermicity of the reaction is substantial, and although Titan's
41 atmosphere is cold, the low densities will limit collisional stabilization of intermediates; therefore
42 most of the isomerization could still be enabled by chemical activation. Because of the numerous
43 intermediates and transition states involved, with multiple product channels, further product
44 detection studies of reactions involving the C_2H radical with C_4H_6 isomers, especially at low
45 temperatures, are required to have a detailed cartography of these radical-molecule reactions.
46
47
48
49
50
51
52
53
54
55
56
57
58
59
60

5. Conclusion

Low temperature rate coefficients (74-295 K) for the $C_2H + 1\text{-butyne}$ reaction are measured in a pulsed Laval nozzle apparatus. In this range, no apparent temperature dependence for the reaction is observed. This behavior is characteristic of a barrierless reaction at rates close to the collision limit, with the formation of an initial excited complex where the C_2H radical adds to the $-C\equiv C-$ group of 1-butyne followed by either elimination of a hydrogen atom or methyl group. At room temperature, using Multiplexed Photoionization Mass Spectrometry, two competing product channels have been identified: $m/z = 64$ (C_5H_4) and $m/z = 78$ (C_6H_6) consistent with the CH_3- and H-loss channels for the reaction respectively. Ethynylallene is identified as the main linear C_5H_4 isomer and is formed in a 4:1 ratio to methyldiacetylene. This result is consistent with the proposed reaction pathways where ethynylallene is most likely formed through a direct β -scission after terminal addition. Interestingly, the C_6H_6 product channel yields cyclic isomers, i.e. fulvene and 3,4-dimethylenecyclobut-1-ene, in almost equal proportions to linear isomers. However, the most stable C_6H_6 isomer, benzene, is most probably not produced in this reaction. Diacetylene formation is also thermodynamically possible, but its presence or absence cannot be ascertained in our experiment. Our results suggests that in the cold, photochemically driven atmosphere of Titan, the formation of linear C_6H_6 isomers should be favored at the expense of cyclic structures due to significant isomerization barriers down the potential energy surface to resonance stabilized structures. The measured rate constants and product branching ratios constitute key laboratory data for the development of chemical schemes in devising more elaborate models for planetary atmospheres, and in particular Titan. Further experimental and theoretical investigations involving the C_2H radical with C_4 carbonaceous species are required to have a detailed cartography of the potential energy surfaces for these reactions.

Acknowledgement

The support of personnel (S.S.) for this research by the National Aeronautics and Space Administration (Grant No. NNX09AB60G) is gratefully acknowledged. We thank Mr. Howard Johnsen for excellent technical support. Sandia authors and instrumentation for this work are supported by the Division of Chemical Sciences, Geosciences and Biosciences, the Office of Basic Energy Sciences, the U.S. Department of Energy. Sandia is a multiprogram laboratory operated by Sandia Corporation, a Lockheed Martin Company, for the National Nuclear Security

1
2
3 Administration under Contract No. DE-AC04-94-AL85000. The Advanced Light Source and
4 Chemical Sciences Division (K.R.W. and S.R.L.) are supported by the Director, Office of
5 Science, Office of Basic Energy Sciences of the U.S. Department of Energy under Contract No.
6 DE-AC02-05CH11231 at the Lawrence Berkeley National Laboratory. A.J.T. acknowledges
7 travel funding provided by the International Synchrotron Access Program (ISAP) managed by the
8 Australian Synchrotron. The ISAP is funded by a National Collaborative Research Infrastructure
9 Strategy grant provided by the Federal Government of Australia.
10
11
12
13
14
15
16
17
18
19
20
21
22
23
24
25
26
27
28
29
30
31
32
33
34
35
36
37
38
39
40
41
42
43
44
45
46
47
48
49
50
51
52
53
54
55
56
57
58
59
60

Bibliography

- (1) Tucker, K. D.; Kutner, M. L.; Thaddeus, P. *Astrophysical Journal* **1974**, *193*, L115.
- (2) Coustenis, A.; Bezdard, B. *Icarus* **1995**, *115*, 126.
- (3) Coustenis, A.; Bezdard, B.; Gautier, D. *Icarus* **1989**, *80*, 54.
- (4) Coustenis, A.; Bezdard, B.; Gautier, D.; Marten, A.; Samuelson, R. *Icarus* **1991**, *89*, 152.
- (5) Seki, K.; Okabe, H. *Journal of Physical Chemistry* **1993**, *97*, 5284.
- (6) Wilson, E. H.; Atreya, S. K. *Planetary and Space Science* **2003**, *51*, 1017.
- (7) Sagan, C.; Khare, B. N.; Thompson, W. R.; McDonald, G. D.; Wing, M. R.; Bada, J. L.; Tuan, V. D.; Arakawa, E. T. *Astrophysical Journal* **1993**, *414*, 399.
- (8) Cook, D. J.; Schlemmer, S.; Balucani, N.; Wagner, D. R.; Steiner, B.; Saykally, R. *J. Nature* **1996**, *380*, 227.
- (9) Snow, T. P.; Le Page, V.; Keheyan, Y.; Bierbaum, V. M. *Nature* **1998**, *391*, 259.
- (10) Coustenis, A.; Achterberg, R. K.; Conrath, B. J.; Jennings, D. E.; Marten, A.; Gautier, D.; Nixon, C. A.; Flasar, F. M.; Teanby, N. A.; Bezdard, B.; Samuelson, R. E.; Carlson, R. C.; Lellouch, E.; Bjoraker, G. L.; Romani, P. N.; Taylor, F. W.; Irwin, P. G. J.; Fouchet, T.; Hubert, A.; Orton, G. S.; Kunde, V. G.; Vinatier, S.; Mondellini, J.; Abbas, M. M.; Courtin, R. *Icarus* **2007**, *189*, 35.
- (11) Mebel, A. M.; Kislov, V. V.; Kaiser, R. I. *Journal of the American Chemical Society* **2008**, *130*, 13618.
- (12) Wang, H.; Frenklach, M. *Combustion and Flame* **1997**, *110*, 173.
- (13) Carty, D.; Le Page, V.; Sims, I. R.; Smith, I. W. M. *Chemical Physics Letters* **2001**, *344*, 310.
- (14) Ceursters, B.; Nguyen, H. M. T.; Peeters, J.; Nguyen, M. T. *Chemical Physics Letters* **2000**, *329*, 412.
- (15) Ceursters, P.; Nguyen, H. M. T.; Peeters, J.; Nguyen, M. T. *Chemical Physics* **2000**, *262*, 243.
- (16) Goulay, F.; Leone, S. R. *Journal of Physical Chemistry A* **2006**, *110*, 1875.
- (17) Goulay, F.; Osborn, D. L.; Taatjes, C. A.; Zou, P.; Meloni, G.; Leone, S. R. *Physical Chemistry Chemical Physics* **2007**, *9*, 4291.
- (18) Hoobler, R. J.; Leone, S. R. *Journal of Geophysical Research-Planets* **1997**, *102*, 28717.
- (19) Hoobler, R. J.; Leone, S. R. *Journal of Physical Chemistry A* **1999**, *103*, 1342.
- (20) Landera, A.; Mebel, A. M.; Kaiser, R. I. *Chemical Physics Letters* **2008**, *459*, 54.
- (21) Lee, S.; Hoobler, R. J.; Leone, S. R. *Review of Scientific Instruments* **2000**, *71*, 1816.
- (22) Lee, S.; Samuels, D. A.; Hoobler, R. J.; Leone, S. R. *Journal of Geophysical Research-Planets* **2000**, *105*, 15085.
- (23) Stahl, F.; Schleyer, P. V.; Bettinger, H. F.; Kaiser, R. I.; Lee, Y. T.; Schaefer, H. F. *Journal of Chemical Physics* **2001**, *114*, 3476.
- (24) Vakhtin, A. B.; Heard, D. E.; Smith, I. W. M.; Leone, S. R. *Chemical Physics Letters* **2001**, *348*, 21.
- (25) Vakhtin, A. B.; Heard, D. E.; Smith, I. W. M.; Leone, S. R. *Chemical Physics Letters* **2001**, *344*, 317.

- 1
2
3 (26) Zhang, F. T.; Kim, S.; Kaiser, R. I. *Physical Chemistry Chemical Physics* **2009**,
4 11, 4707.
5 (27) Krasnopolsky, V. A. *Icarus* **2009**, 201, 226.
6 (28) Yung, Y. L.; Allen, M.; Pinto, J. P. *Astrophysical Journal Supplement Series* **1984**,
7 55, 465.
8 (29) Hebrard, E.; Dobrijevic, M.; Benilan, Y.; Raulin, F. *Journal of Photochemistry*
9 *and Photobiology C-Photochemistry Reviews* **2006**, 7, 211.
10 (30) Hansmann, B.; Abel, B. *Chemphyschem* **2007**, 8, 343.
11 (31) Dupeyrat, G.; Marquette, J. B.; Rowe, B. R. *Physics of Fluids* **1985**, 28, 1273.
12 (32) Rowe, B. R.; Dupeyrat, G.; Marquette, J. B.; Gaucherel, P. *Journal of Chemical*
13 *Physics* **1984**, 80, 4915.
14 (33) Chastaing, D.; James, P. L.; Sims, I. R.; Smith, I. W. M. *Faraday Discussions*
15 **1998**, 109, 165.
16 (34) James, P. L.; Sims, I. R.; Smith, I. W. M.; Alexander, M. H.; Yang, M. B. *Journal*
17 *of Chemical Physics* **1998**, 109, 3882.
18 (35) Sims, I. R.; Smith, I. W. M. *Annual Review of Physical Chemistry* **1995**, 46, 109.
19 (36) Atkinson, D. B.; Jaramillo, V. I.; Smith, M. A. *Journal of Physical Chemistry A*
20 **1997**, 101, 3356.
21 (37) Atkinson, D. B.; Smith, M. A. *Journal of Physical Chemistry* **1994**, 98, 5797.
22 (38) Berteloite, C.; Le Picard, S. D.; Birza, P.; Gazeau, M. C.; Canosa, A.; Benilan, Y.;
23 Sims, I. R. *Icarus* **2008**, 194, 746.
24 (39) Nizamov, B.; Leone, S. R. *Journal of Physical Chemistry A* **2004**, 108, 1746.
25 (40) Vuitton, V.; Doussin, J. F.; Benilan, Y.; Raulin, F.; Gazeau, M. C. *Icarus* **2006**,
26 185, 287.
27 (41) Vuitton, V.; Yelle, R. V.; Cui, J. *Journal of Geophysical Research-Planets* **2008**,
28 113, 18.
29 (42) Lavvas, P. P.; Coustenis, A.; Vardavas, I. M. *Planetary and Space Science* **2008**,
30 56, 27.
31 (43) Lavvas, P. P.; Coustenis, A.; Vardavas, I. M. *Planetary and Space Science* **2008**,
32 56, 67.
33 (44) Hansen, N.; Miller, J. A.; Kasper, T.; Kohse-Hoinghaus, K.; Westmoreland, P. R.;
34 Wang, J.; Cool, T. A. *Proceedings of the Combustion Institute* **2009**, 32, 623.
35 (45) Vanlook, H.; Peeters, J. *Journal of Physical Chemistry* **1995**, 99, 16284.
36 (46) Montgomery, J. A.; Frisch, M. J.; Ochtanski, J. W.; Petersson, G. A. *Journal of*
37 *Chemical Physics* **1999**, 110, 2822.
38 (47) Montgomery, J. A.; Frisch, M. J.; Ochtanski, J. W.; Petersson, G. A. *Journal of*
39 *Chemical Physics* **2000**, 112, 6532.
40 (48) Ervin, K. M., PESCAL, Fortran program, 2009.
41 (49) Ervin, K. M.; Ramond, T. M.; Davico, G. E.; Schwartz, R. L.; Casey, S. M.;
42 Lineberger, W. C. *Journal of Physical Chemistry A* **2001**, 105, 10822.
43 (50) Osborn, D. L.; Zou, P.; Johnsen, H.; Hayden, C. C.; Taatjes, C. A.; Knyazev, V.
44 D.; North, S. W.; Peterka, D. S.; Ahmed, M.; Leone, S. R. *Review of Scientific Instruments* **2008**,
45 79.
46 (51) Slagle, I. R.; Yamada, F.; Gutman, D. *Journal of the American Chemical Society*
47 **1981**, 103, 149.
48 (52) Meloni, G.; Selby, T. M.; Goulay, F.; Leone, S. R.; Osborn, D. L.; Taatjes, C. A.
49 *Journal of the American Chemical Society* **2007**, 129, 14019.
50
51
52
53
54
55
56
57
58
59
60

- 1
2
3 (53) Minsek, D. W.; Chen, P. *Journal of Physical Chemistry* **1990**, *94*, 8399.
4 (54) Bieri, G.; Burger, F.; Heilbronner, E.; Maier, J. P. *Helvetica Chimica Acta* **1977**,
5 60, 2213.
6 (55) Kiess, N. H.; Broida, H. P. *Astrophysical Journal* **1956**, *123*, 166.
7 (56) Cvejanovic, D.; Adams, A.; King, G. C. *Journal of Physics B-Atomic Molecular*
8 *and Optical Physics* **1978**, *11*, 1653.
9 (57) Sander, R. K.; Tsee, J. J.; Quick, C. R.; Romero, R. J. *Journal of Chemical Physics*
10 **1988**, *89*, 3495.
11 (58) Nakayama, T.; Watanabe, K. *Journal of Chemical Physics* **1964**, *40*, 558.
12 (59) Laufer, A. H.; Fahr, A. *Chem. Rev.* **2004**, *104*, 2813.
13 (60) Berkowitz, J.; Ellison, G. B.; Gutman, D. *Journal of Physical Chemistry* **1994**, *98*,
14 2744.
15 (61) Miller, J. A.; Klippenstein, S. J. *Journal of Physical Chemistry A* **2003**, *107*, 7783.
16 (62) Hansen, N.; Klippenstein, S. J.; Miller, J. A.; Wang, J.; Cool, T. A.; Law, M. E.;
17 Westmoreland, P. R.; Kasper, T.; Kohse-Hoinghaus, K. *Journal of Physical Chemistry A* **2006**,
18 *110*, 4376.
19 (63) Bobeldijk, M.; Vanderzande, W. J.; Kistemaker, P. G. *Chemical Physics* **1994**,
20 *179*, 125.
21 (64) Fahr, A.; Selby, T. M.; Osborn, D. L.; Taatjes, C. A. private communication, 2006.
22 (65) Nemeth, G. I.; Selzle, H. L.; Schlag, E. W. *Chemical Physics Letters* **1993**, *215*,
23 151.
24 (66) Rosenstock, H. M.; Dannacher, J.; Liebman, J. F. *Radiation Physics and*
25 *Chemistry* **1982**, *20*, 7.
26 (67) Masclet, P.; Mouvier, G.; Bocquet, J. F. *Journal De Chimie Physique Et De*
27 *Physico-Chimie Biologique* **1981**, *78*, 99.
28 (68) Beez, M.; Bieri, G.; Bock, H.; Heilbron, E. *Helvetica Chimica Acta* **1973**, *56*, 1028.
29 (69) Goulay, F.; Rebrion-Rowe, C.; Biennier, L.; Le Picard, S. D.; Canosa, A.; Rowe,
30 B. R. *Journal of Physical Chemistry A* **2006**, *110*, 3132.
31 (70) Herbst, E.; Woon, D. E. *Astrophysical Journal* **1997**, *489*, 109.
32 (71) Senosiain, J. P.; Miller, J. A. *Journal of Physical Chemistry A* **2007**, *111*, 3740.
33 (72) Matheu, D. M.; Green, W. H.; Grenda, J. M. *International Journal of Chemical*
34 *Kinetics* **2003**, *35*, 95.
35 (73) Laufer, A. H.; Fahr, A. *Chemical Reviews* **2004**, *104*, 2813.
36 (74) Woon, D. E.; Park, J. Y. *Icarus* **2009**, *202*, 642.
37 (75) Maier, J. P. *Angewandte Chemie-International Edition in English* **1981**, *20*, 638.
38 (76) Hayaishi, T.; Iwata, S.; Sasanuma, M.; Ishiguro, E.; Morioka, Y.; Iida, Y.;
39 Nakamura, M. *Journal of Physics B-Atomic Molecular and Optical Physics* **1982**, *15*, 79.
40
41
42
43
44
45
46
47
48
49
50
51
52
53
54
55
56
57
58
59
60

Captions for Figures:

Figure 1: (a) Example of net CH ($A^2\Delta - X^2\Pi_r$) chemiluminescence decay signal at 431.22 nm⁵⁶ on a linear scale, and (b) a semi-logarithmic scale. The solid black line is the single exponential fit of the signal within the range 15 – 200 μ s as indicated by the dashed line. The chemiluminescence signal is proportional to the concentration of ethynyl radicals (C_2H) under the experimental conditions.

Figure 2: Plot of the pseudo first order rate constant (k_{obs}) as a function of the density of 1-butyne inside the flow at 84 K and 0.3 Torr. The black line is a least squares fit to the experimental values. The error bars are given as $\pm 2\sigma$ of the single exponential fits for each concentration.

Figure 3: Mass spectra at 10.1 eV photoionization energy with (a) the C_2H precursor and 1-butyne and (b) only 1-butyne flowing under the same exact conditions. Two masses show a significant rise as the C_2H precursor is added, i.e. $m/z = 64$ and $m/z = 78$ which are consistent with the CH_3 - and H-loss channels of the reaction respectively. The contribution of the 193 nm photoproducts of 1-butyne to the $m/z = 78$ product channel of the reaction is discussed in Section 3.2.1. Note that the contribution to the ion signal at $m/z = 66$ (\star) is due to the reaction of the ethynyl radical with butene (C_4H_8) present as a small contaminant in the flow.

Figure 4: Photoionization efficiency curves for $m/z = 78$ (C_6H_6) mass channel with (\blacklozenge) and without (\otimes) the C_2H precursor. Both PIE curves have been recorded with the same concentration of 1-butyne in the total gas flow. The photodissociation of 1-butyne at 193 nm produces propargyl radicals (C_3H_3) that subsequently react with 1-butyne to form $C_6H_6 + CH_3$. In presence of C_2H radicals, the ion signal is enhanced (typically by a factor of ~ 6) which is consistent with the formation of C_6H_6 as a product of the reaction of C_2H radicals with 1-butyne. Two thresholds are identified and indicated by dashed arrows: (A) around 8.8 eV photoionization energy as shown in the region between 8.1 and 8.9 eV (zoom x8) and (B) around 9.4 eV. The identification of the different isomers C_6H_6 is discussed in Section 3.2.3.

1
2
3
4
5 Figure 5: Measurements of the photodepletion of (a) 1-butyne, (b) acetylene and (c) 3,3,3-
6 trifluoropropyne at 193 nm. All gases are seeded in He buffer gas at the following compositions:
7 0.1 % for both 1-butyne and acetylene and 1% for 3,3,3-trifluoropropyne. The excimer laser
8 energy used for the three different species is typically ~ 27 mJ/cm². All data sets are fit by a step
9 function (solid black line) after the laser is pulsed at 20 ms. The percentage depletion is reported
10 in Table 4.
11
12
13
14
15
16

17 Figure 6: Photoionization efficiency curve (\oplus) of $m/z = 78$ product ion. The individual
18 contributions of the C₆H₆ isomers (dotted and dashed lines) are shown, as well as the cumulative
19 simulation (thick black line). The adiabatic ionization energies for each isomer are also labeled:
20 (a) fulvene, (b) DMCB, (c) 2-ethynyl-1,3-butadiene, 3,4-hexadiene-1-yne and (d) 1,3-hexadiyne.
21 The production of the aromatic 6-membered ring isomer, benzene, is most probably negligible as
22 no sharp characteristic onset is observed around 9.23 eV (see Section 3.2.3). The PIE curve is
23 normalized to the total estimated cross section of an average mixture of 18% of fulvene, 32% of
24 DMCB, 8% of 2-ethynyl-1,3-butadiene, 28% of 3,4-hexadiene-1-yne and 14% of 1,3-hexadiyne
25 using the estimated photoionization cross sections at 10 eV reported in Table 6.
26
27
28
29
30
31
32
33

34 Figure 7: Photoionization efficiency curve (\oplus) of $m/z = 64$. Note that no threshold in the ion
35 signal is observed at 8.67 eV, indicating that no 1,2,3,4-pentatetraene is produced in the reaction.
36 (a) A single contribution of ethynylallene cannot account for the observed ion signal in the 8.2 –
37 10.1 photon range. (b) The individual contributions of ethynylallene (dashed line) and
38 methyldiacetylene (dotted line) are shown. The ion signal can be fit by a sum of weighted
39 contributions of Franck-Condon simulations⁶² at 300 K of the two most stable C₅H₄ isomers as
40 shown by the thick black line. The calculated PIE curve of 1,4-pentadiyne (gray dashed line) is
41 also indicated. Due to experimental limitations, the presence or absence of 1,4-pentadiyne (IE =
42 10.27 eV)⁶² cannot be probed. The signal is normalized to the total estimated photoionization
43 cross section at 9.8 eV using estimated values reported in Table 5.
44
45
46
47
48
49
50
51
52
53
54
55
56
57
58
59
60

1
2
3 Figure 8: Comparison between the measured rate constant for the reactions of the ethynyl radical
4 with 1-butyne (^athis work) and the smaller alkynes: propyne (^bLeone and coworkers²⁵ and ^cSims
5 and coworkers¹³) and acetylene (^dLeone and coworkers²⁴ and ^eSims and coworkers³³).
6
7
8
9

10 Figure 9: A comparison of the thermochemistry of the $C_3H_3 + C_3H_3$ and $C_2H + 1$ -butyne
11 reactions. The standard heats of reaction (kcal/mol) leading to the three most stable C_6H_6
12 isomers, i.e. DMCB, fulvene and benzene respectively are shown in both cases. The difference in
13 internal energy accompanying benzene is ~ 38 kcal/mol. The exothermicity of the CH_3 - and C_2H_5 -
14 loss channels forming methyldiacetylene (CH_3CCCCH) and diacetylene ($HCCCCH$) respectively
15 is also shown.
16
17
18
19
20
21

22 Figure 10: Proposed reaction pathways following addition of C_2H radical (shown in bold
23 characters) to the terminal acetylenic carbon atom in 1-butyne. The initial adduct formed is
24 shown inside the rectangular frame.
25
26
27
28

29 Figure 11: Proposed reaction pathways following addition of the C_2H radical (shown in bold
30 characters) to the central acetylenic carbon atom in 1-butyne. The initial adduct formed is shown
31 inside the rectangular frame.
32
33
34
35
36
37
38
39
40
41
42
43
44
45
46
47
48
49
50
51
52
53
54
55
56
57
58
59
60

Captions for Tables:

Table 1: Isomers of C_6H_6 relevant to this work and their ionization energies.

Table 2: Isomers of C_5H_4 relevant to this work and their ionization energies.

Table 3: Low temperature rate coefficients of the reaction of the ethynyl radical (C_2H) with 1-butyne (C_4H_6) obtained with the pulsed Laval nozzle apparatus. The values are given with a total uncertainty of 20%.

Table 4: Percent photo-depletion of acetylene, 3,3,3-trifluoropropyne and 1-butyne at 193 nm at a laser energy ~ 27 mJ/pulse. The experimental data is fit to a step function after the laser is pulsed, i.e. at $t = 20$ ms (see Figure 5 and Section 3.2.1).

Table 5: Estimated photoionization absorption cross sections of C_5H_4 isomers identified in the PIE curve shown in Figure 7 (see Section 3.2.2).

Table 6: Estimated photoionization absorption cross sections of C_6H_6 isomers (see Section 3.2.3) identified in the PIE curve shown in Figure 6.

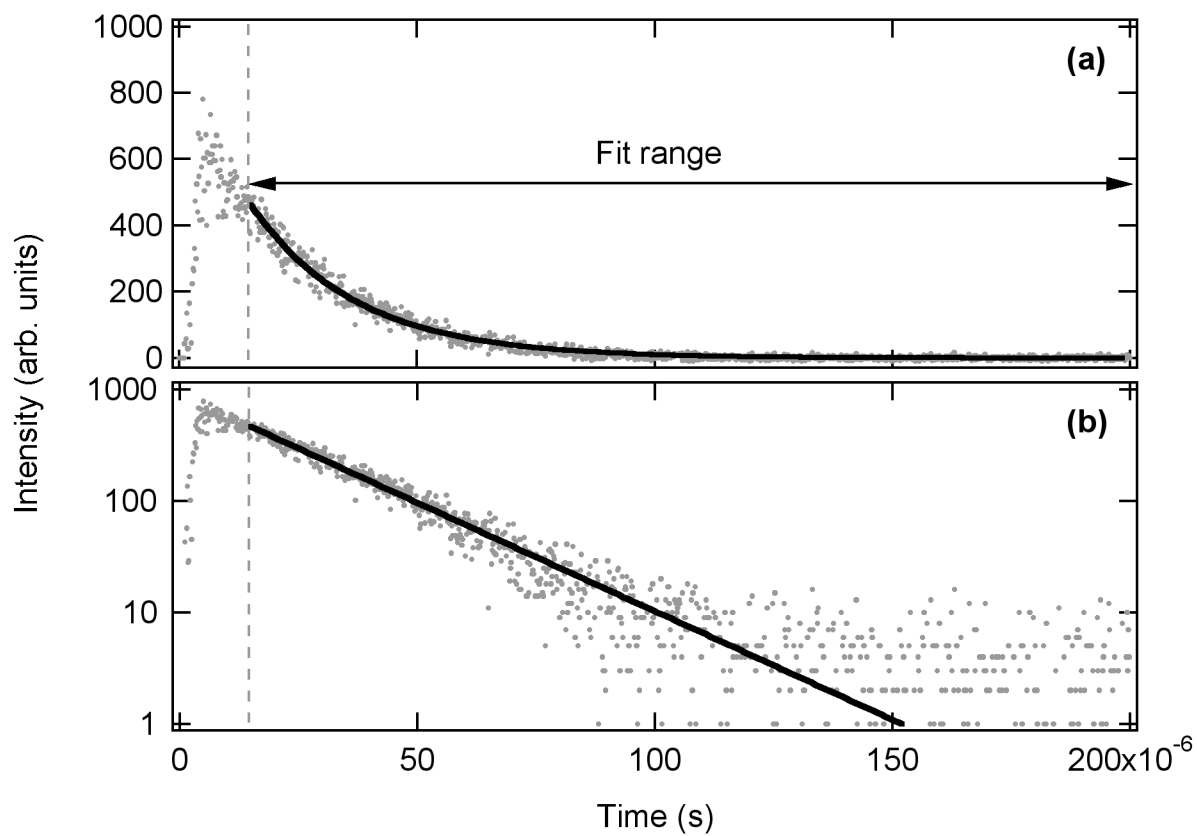


Figure 1

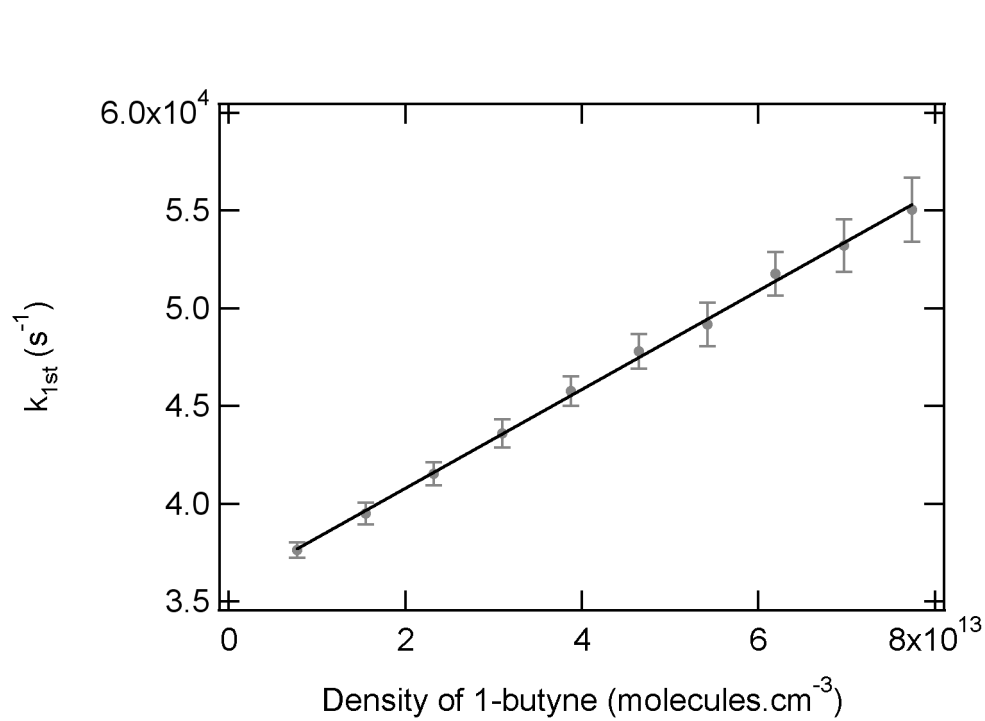


Figure 2

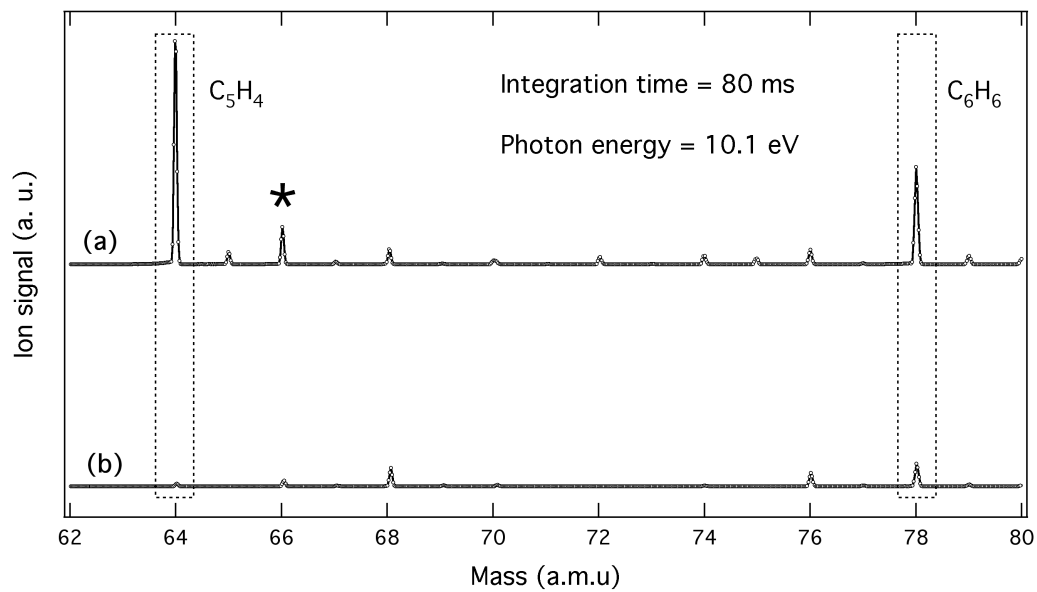


Figure 3

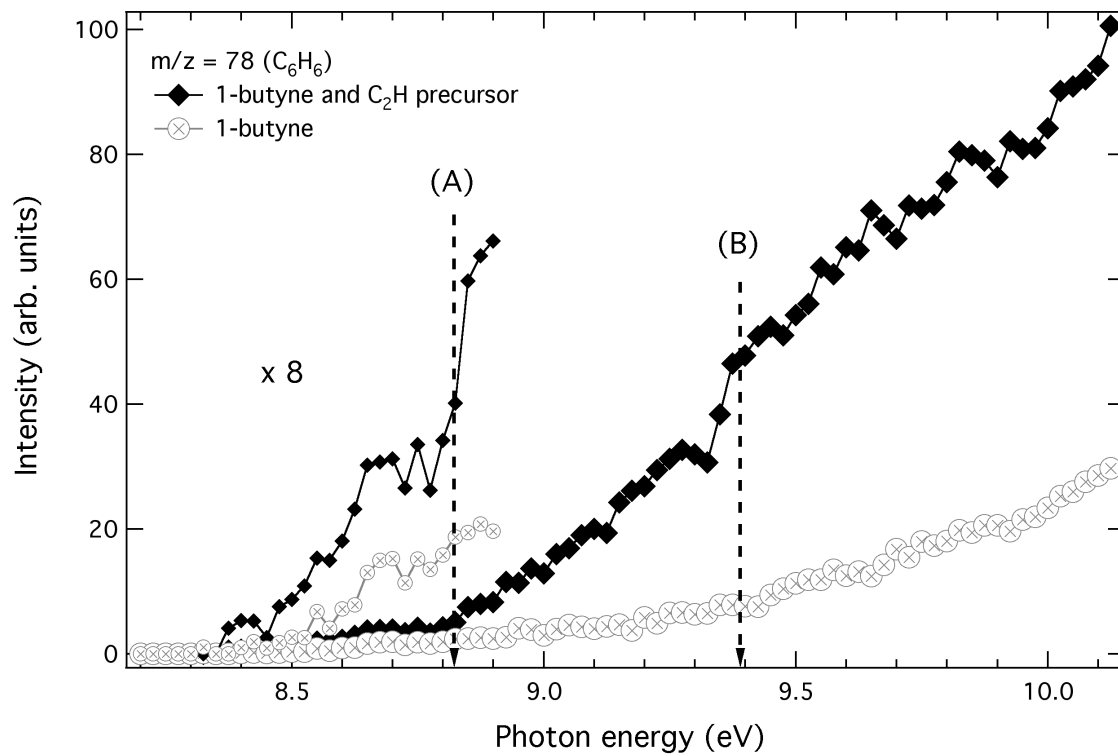


Figure 4

28
29
30
31
32
33
34
35
36
37
38
39
40
41
42
43
44
45
46
47
48
49
50
51
52
53
54
55
56
57
58
59
60

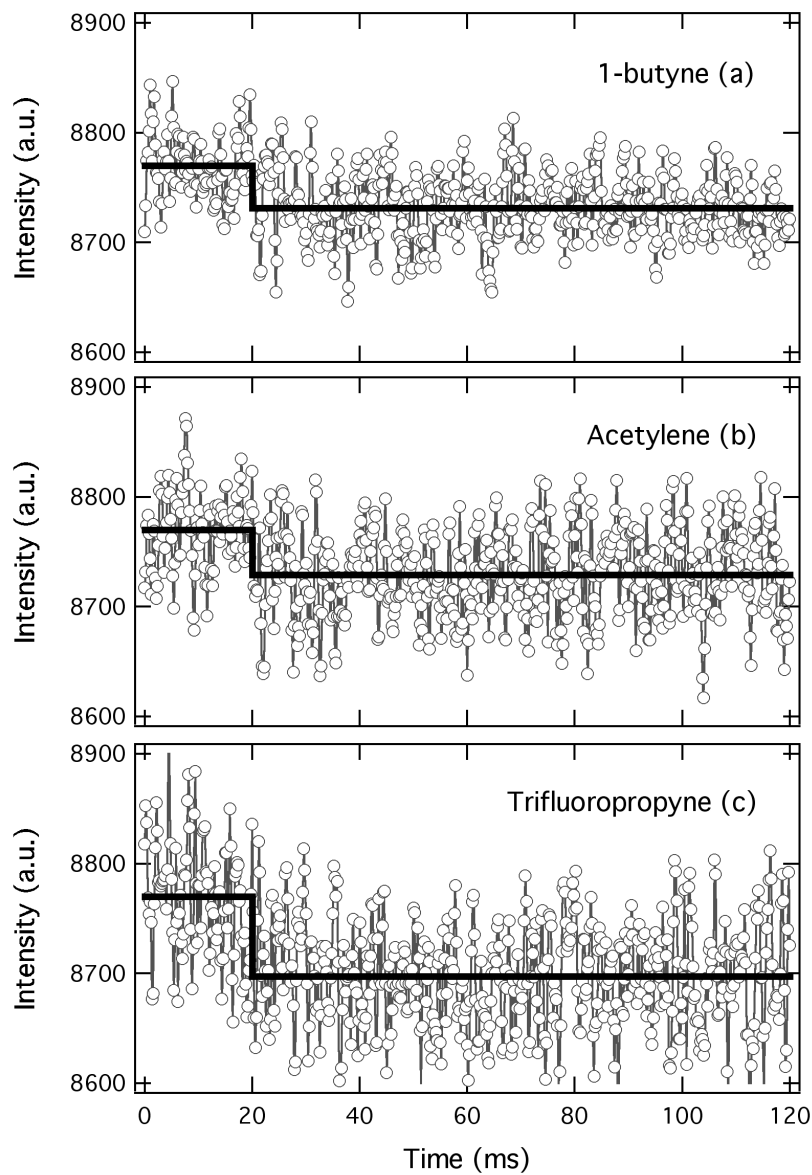


Figure 5

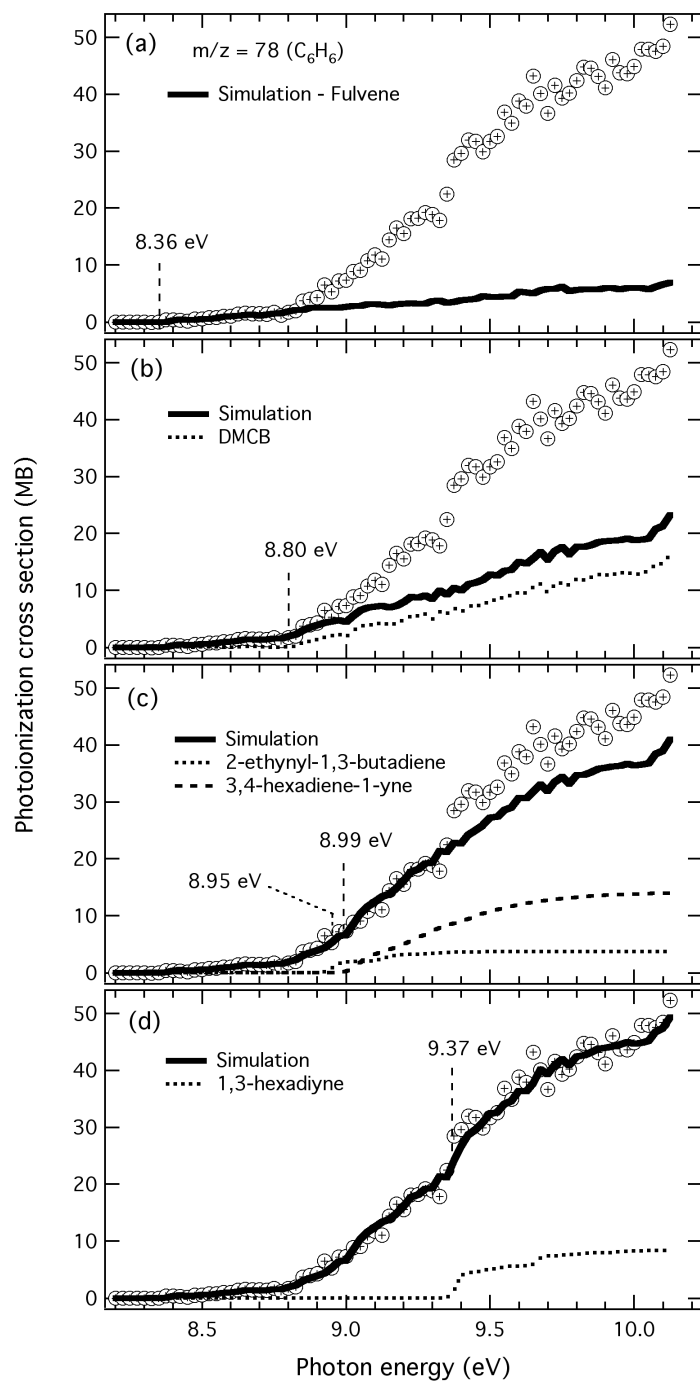


Figure 6

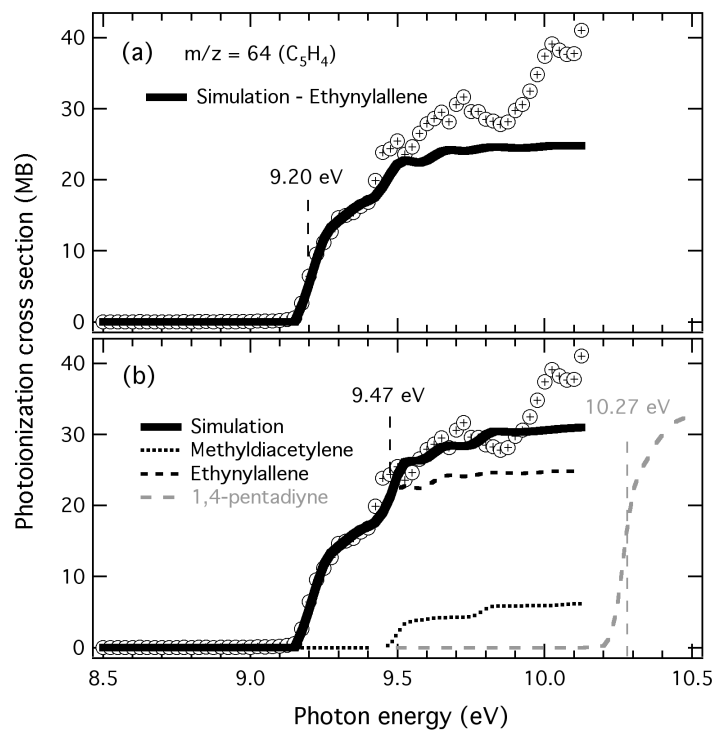


Figure 7

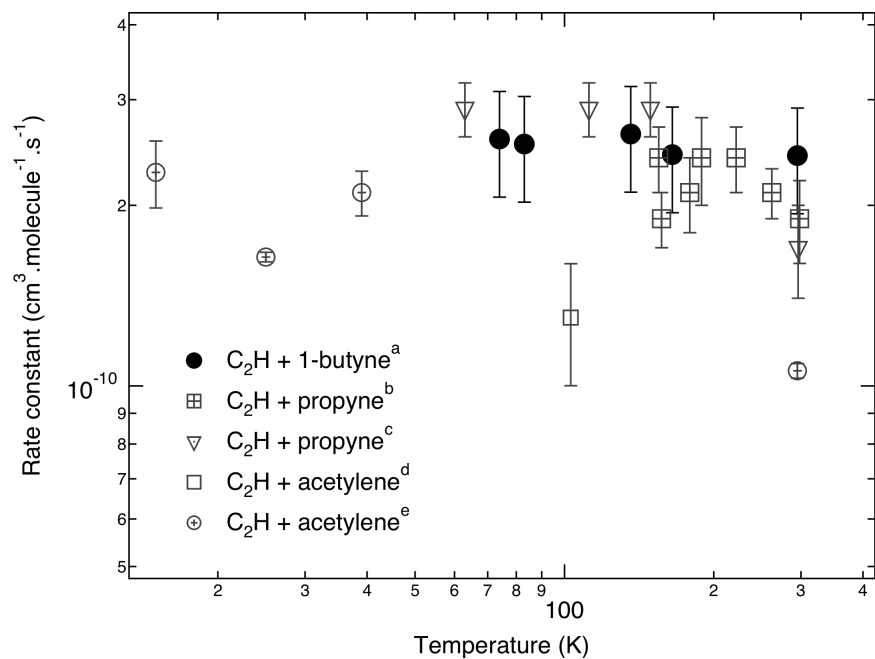


Figure 8

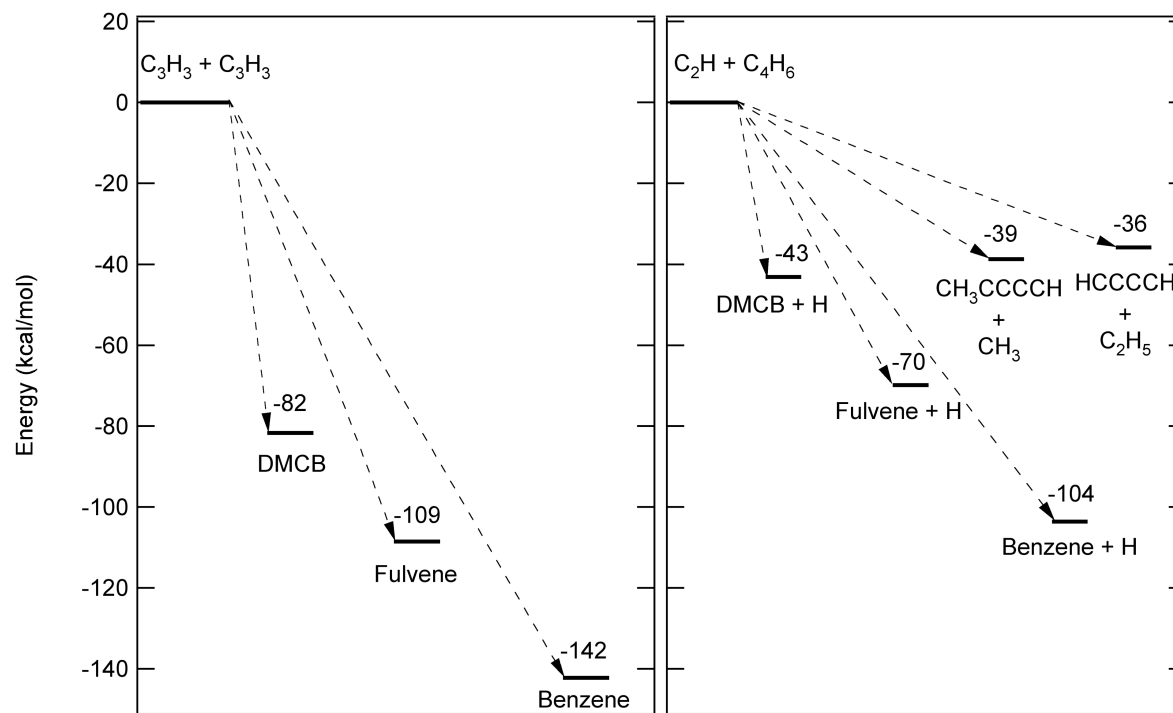


Figure 9

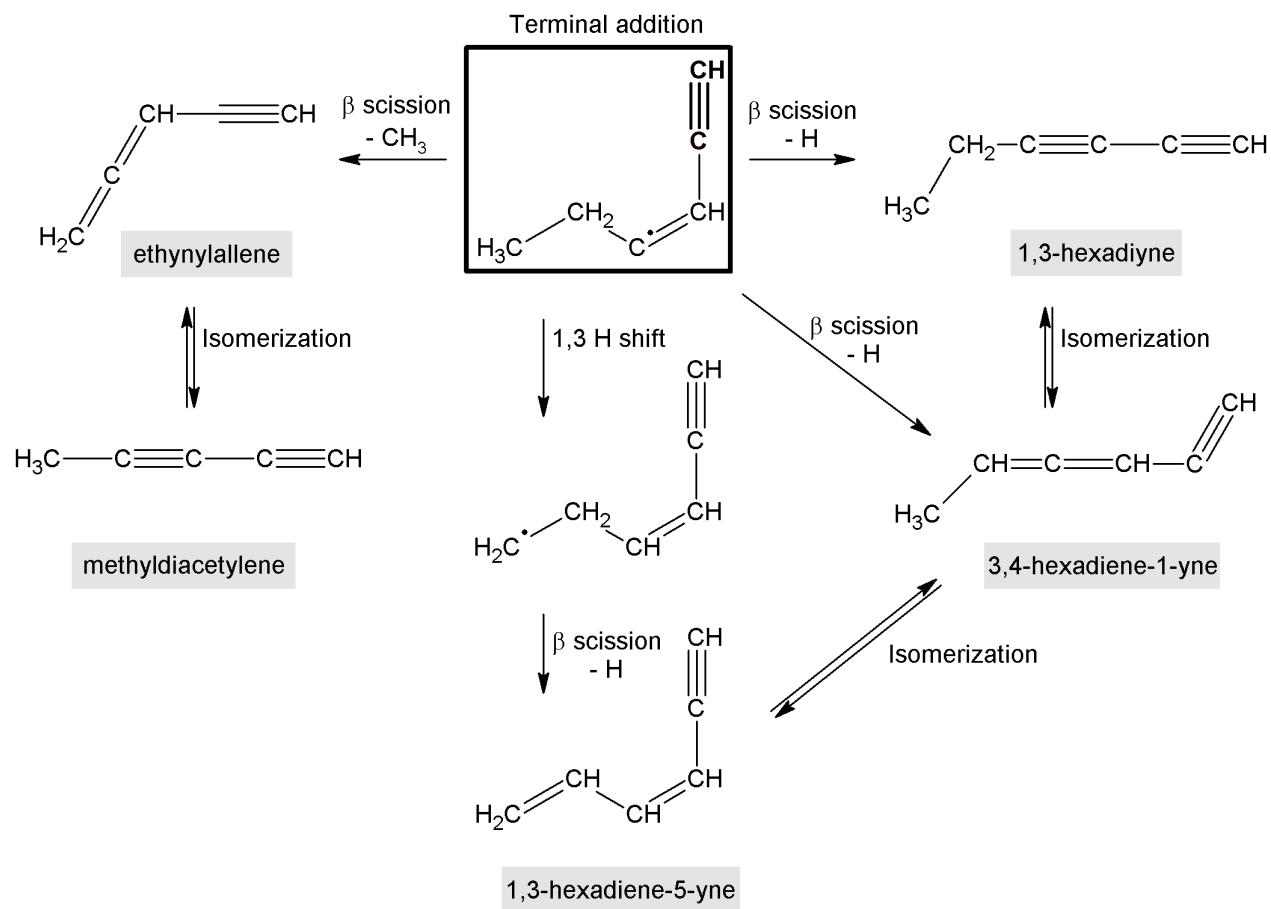


Figure 10

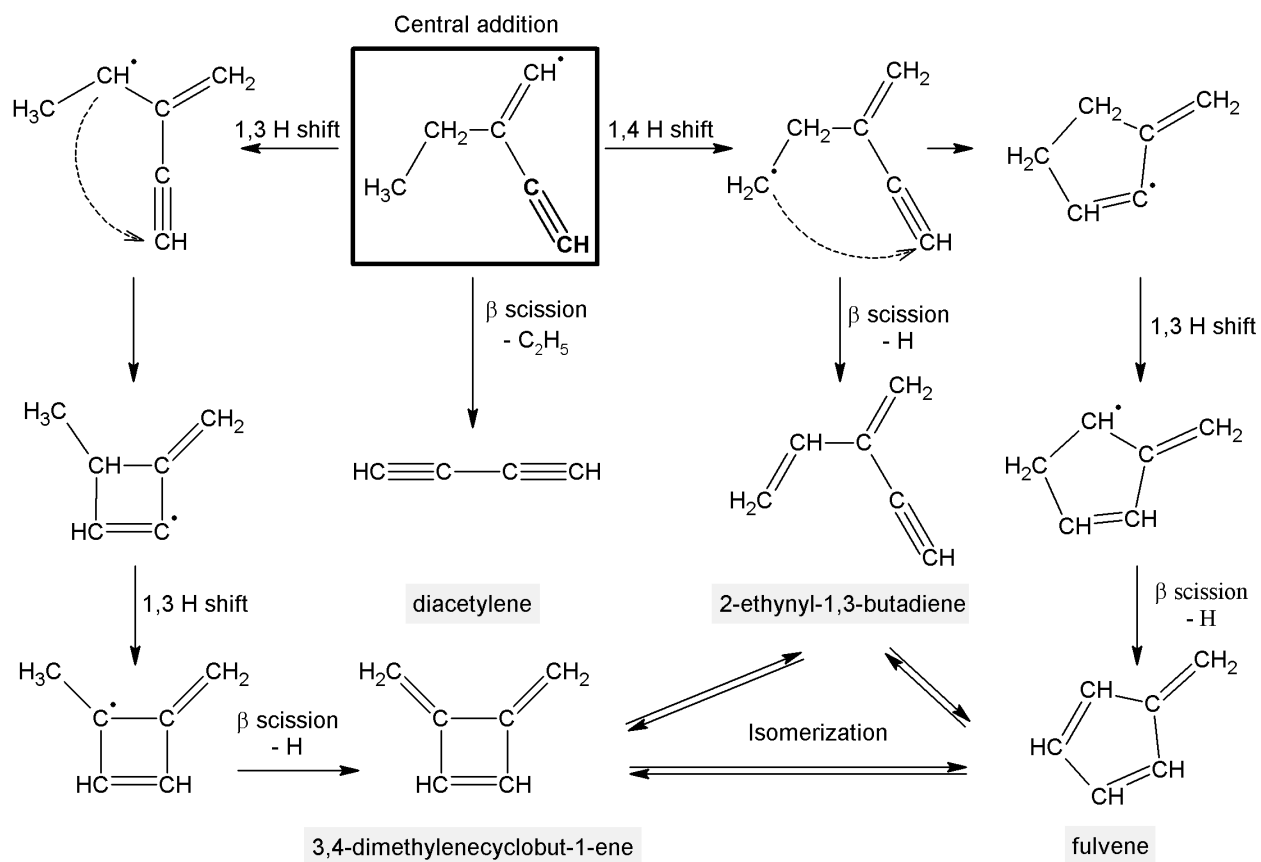
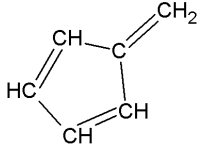
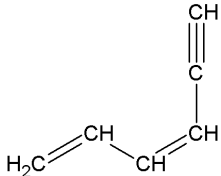
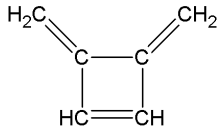
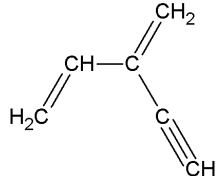
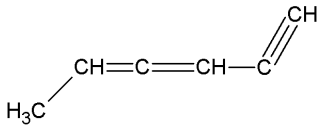
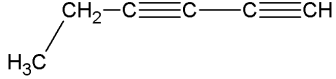
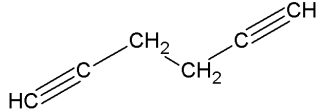


Figure 11

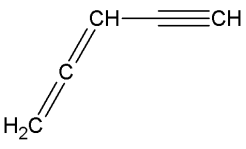
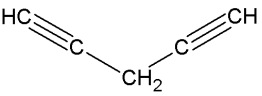
33
34
35
36
37
38
39
40
41
42
43
44
45
46
47
48
49
50
51
52
53
54
55
56
57
58
59
60

Table 1

Name	Molecular structure	Ionization energies (eV)	
		Calc. ^a	Exp.
Fulvene		8.40	8.36 ^b
1,3-hexadiene-5-yne		8.63	9.2 ^{c,d}
DMCB		8.75	8.80 ^b
2-ethynyl-1,3-butadiene		8.95	
3,4-hexadiene-1-yne		8.99	
1,3-hexadiyne		9.37	9.41 ^c
1,5-hexadiyne		9.90	9.90 ^b

^aThis work, CBS-QB3 calculations^bRef.⁵⁴^cRef.⁶⁶^dElectron impact value minus 0.3 eV as reported in Ref.⁶⁶

Table 2

Name	Molecular structure	Ionization energies (eV)	
		Calc. ^a	Lit.
1,2,3,4-pentatetraene	$\text{H}_2\text{C}=\text{C}=\text{C}=\text{C}=\text{CH}_2$		8.67 ^b
ethynylallene		9.20	9.22 ^c
methyldiacetylene	$\text{H}_3\text{C}-\text{C}\equiv\text{C}-\text{C}\equiv\text{CH}$	9.47	9.5 ^d
1,4-pentadiyne		10.27	10.28 ^c

^aThis work, CBS-QB3 calculations^bRef.⁵⁴^cRef.⁶²^dRef.⁷⁵

Table 3

T (K)	Total gas density (10^{16} cm^{-3})	[C ₂ H ₂] (10^{14} cm^{-3})	[O ₂] (10^{14} cm^{-3})	[1-butyne] (10^{12} cm^{-3})	Rate constant ($10^{-10} \text{ cm}^3 \text{ s}^{-1}$)
74	2.1	1.2	2.3	4.6 – 46	2.58±0.5
84	3.6	2.0	3.9	7.8 – 77	2.53±0.5
136	5.6	3.5	7.0	14 – 136	2.63±0.5
165	4.6	4.8	4.8	7.5 – 194	2.43±0.5
295	3.2	3.8	3.8	4.0 – 40	2.42±0.5

Table 4

Molecule	Formula	IE (eV)	% in He buffer gas	% depletion
acetylene	C ₂ H ₂	11.40 ⁷⁶	0.1	0.47
3,3,3-trifluoropropyne	CF ₃ C ₂ H	11.96 ⁵⁴	1.0	0.83
1-butyne	C ₄ H ₆	10.20 ⁵⁴	0.1	0.45

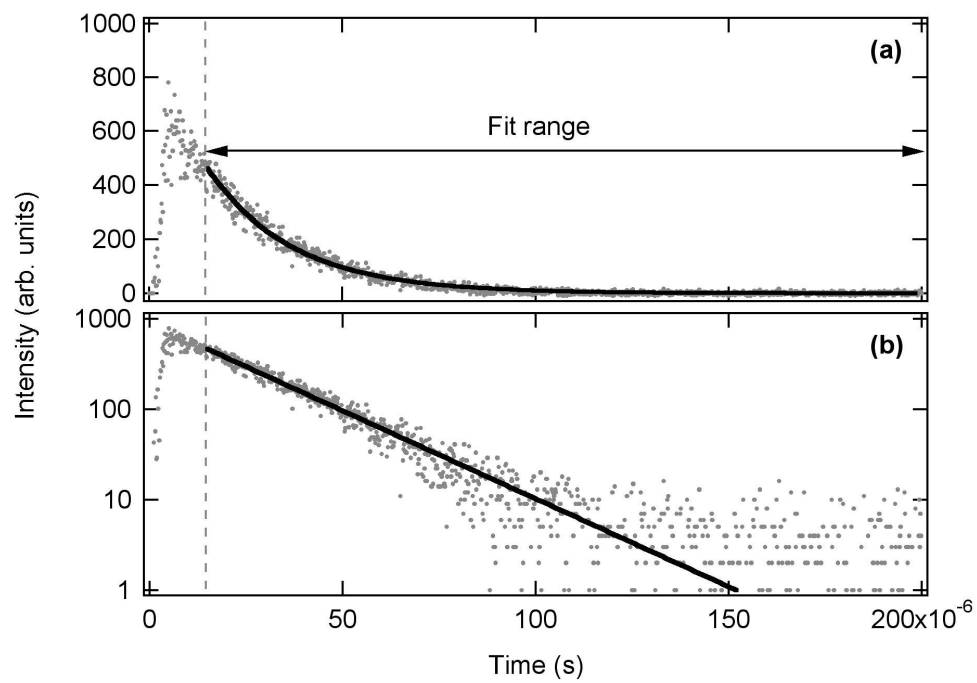
Table 5

C ₅ H ₄ isomers	Photon energy (eV)		
	9.4	9.8	10.4
ethynylallene ^a	25 MB	30 MB	30 MB
methyldiacetylene ^a		30 MB	35 MB
1,4-pentadiyne ^a			30 MB

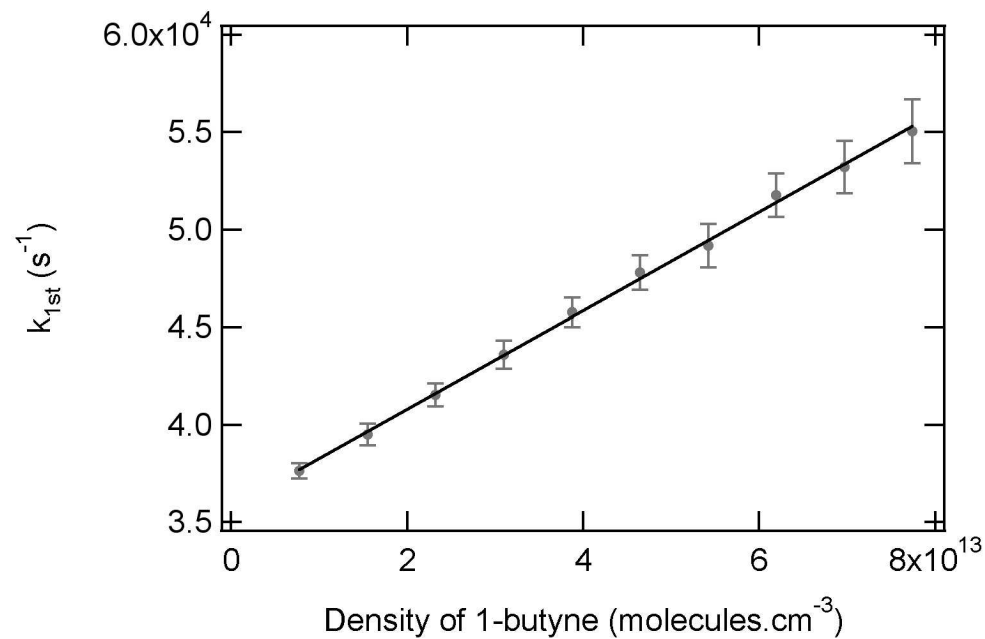
^aRef.¹⁷

Table 6

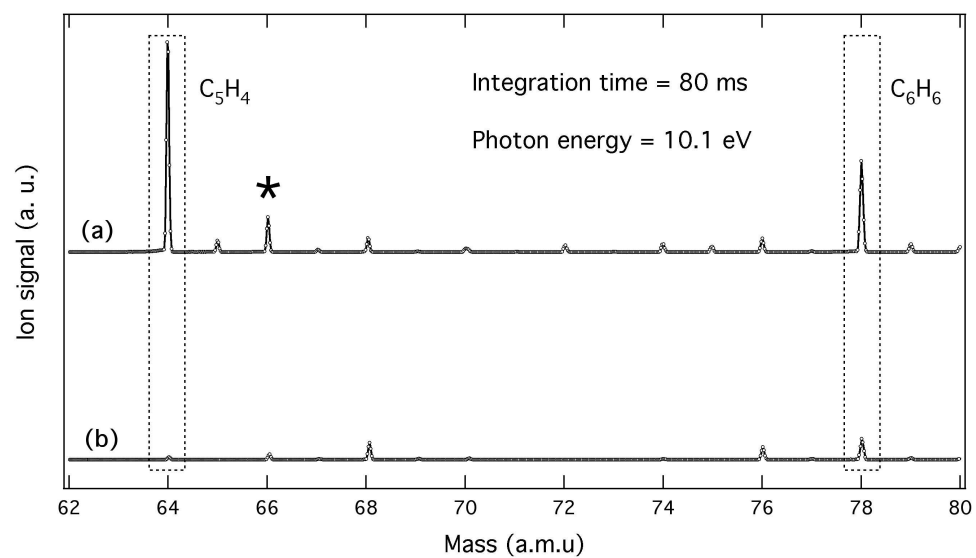
C ₆ H ₆ isomers	Photon energy (eV)			
	8.6	8.9	9.2	10
fulvene	6 MB	14 MB	18 MB	35 MB
3,4-dimethylenecyclobut-1-ene		5 MB	15 MB	40 MB
2-ethynyl-1,3-butadiene			42 MB	50 MB
3,4-hexadiene-1-yne			18 MB	50 MB
1,3-hexadiyne				59 MB



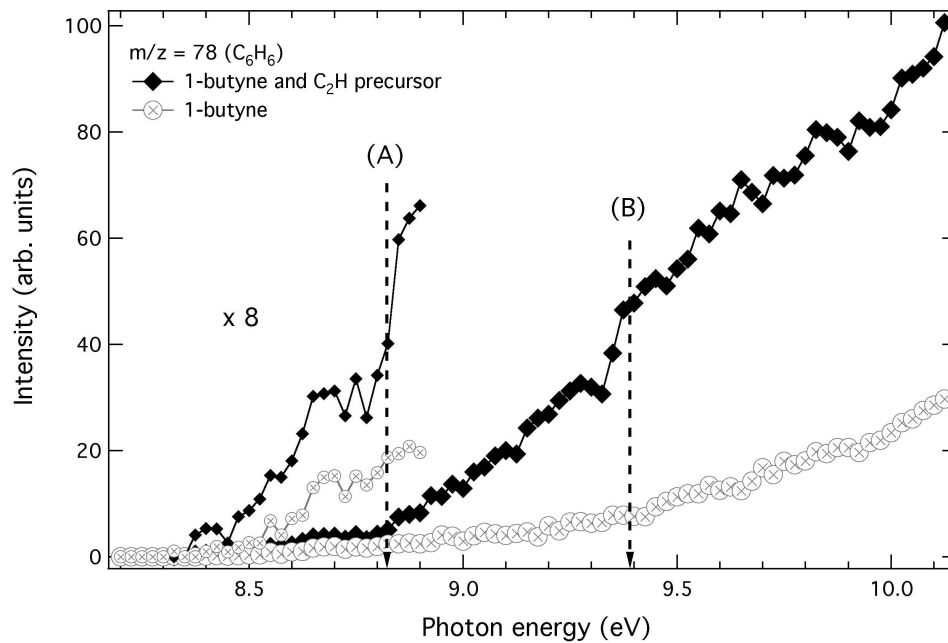
162x114mm (300 x 300 DPI)



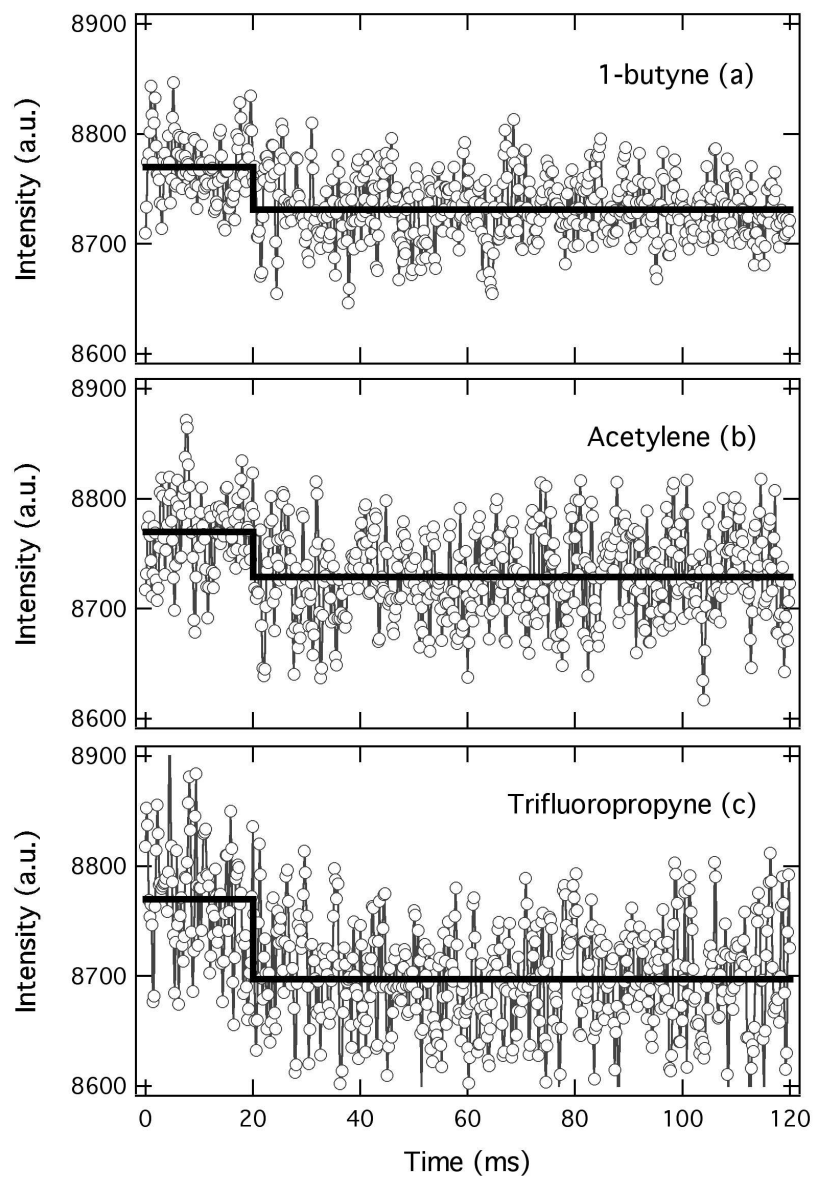
132x84mm (300 x 300 DPI)



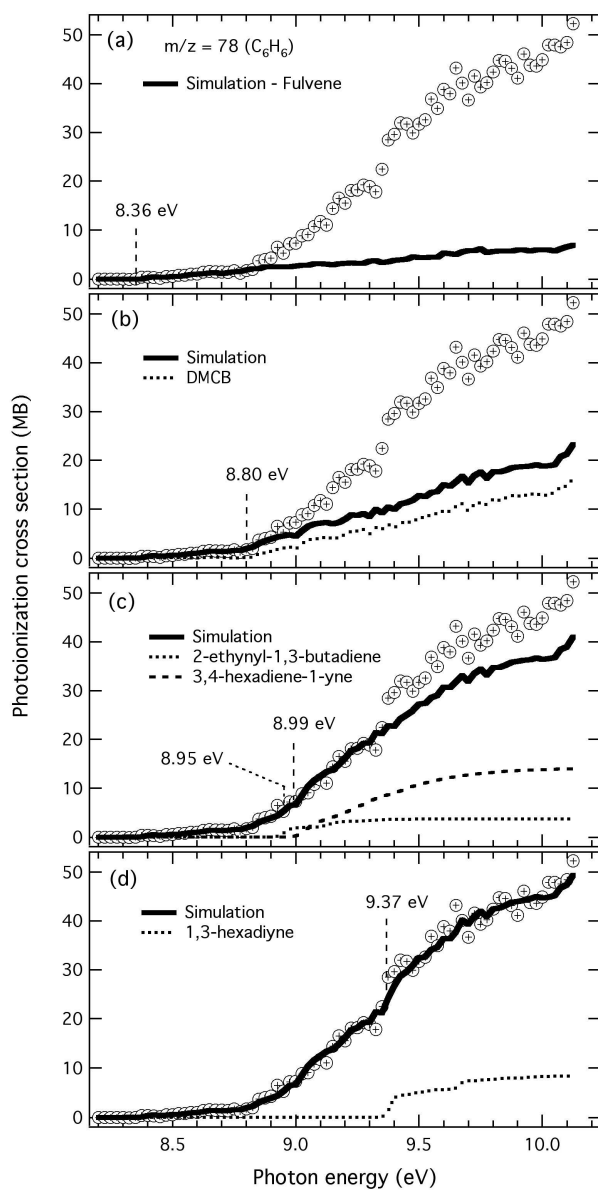
234x131mm (300 x 300 DPI)



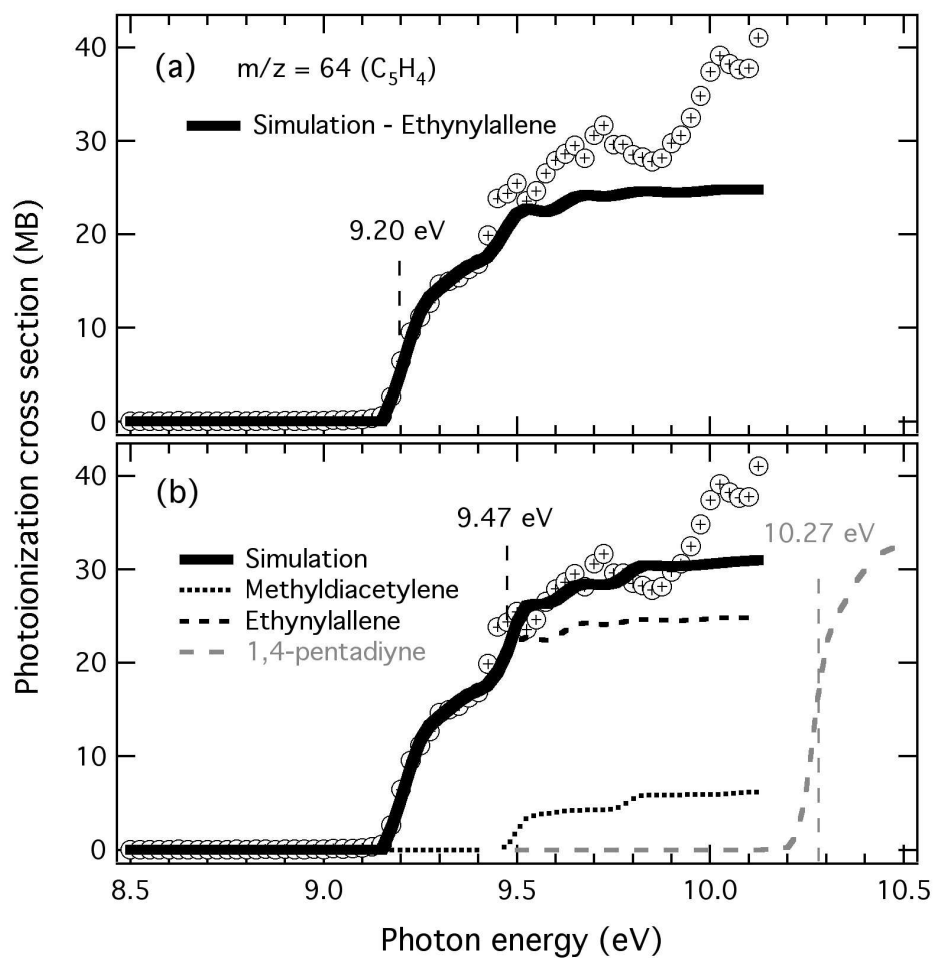
221x142mm (300 x 300 DPI)



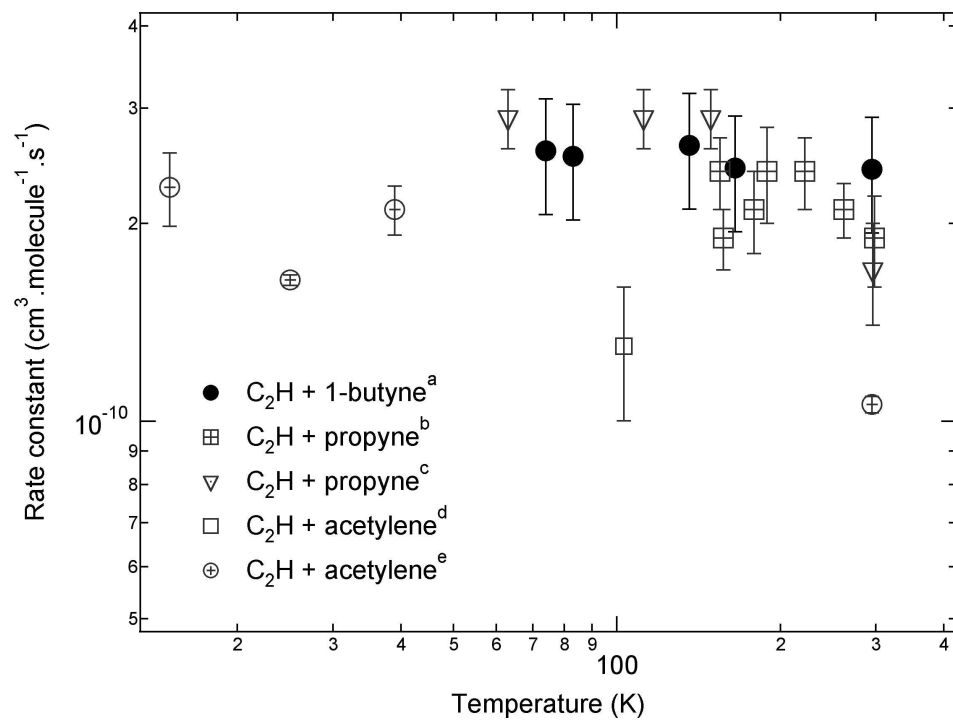
143x198mm (300 x 300 DPI)



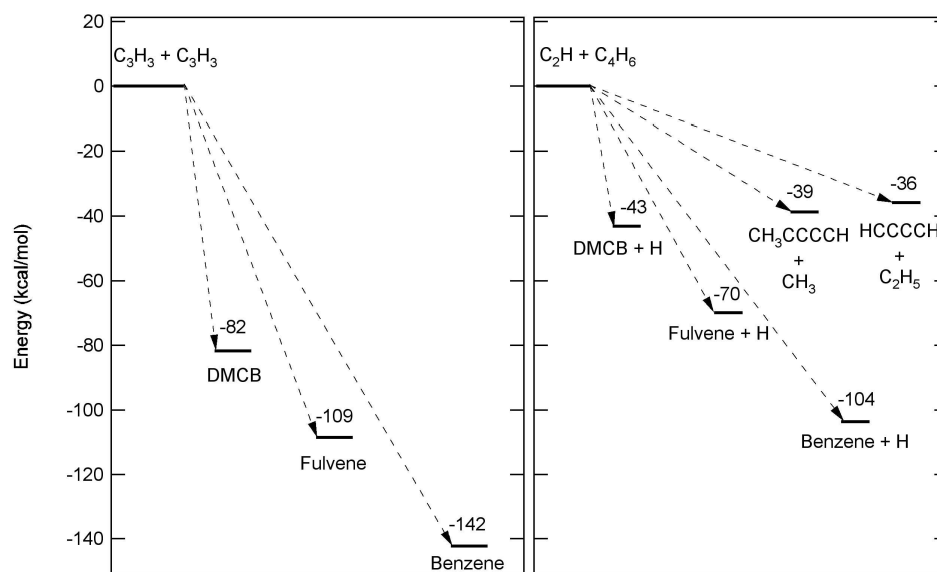
143x263mm (300 x 300 DPI)



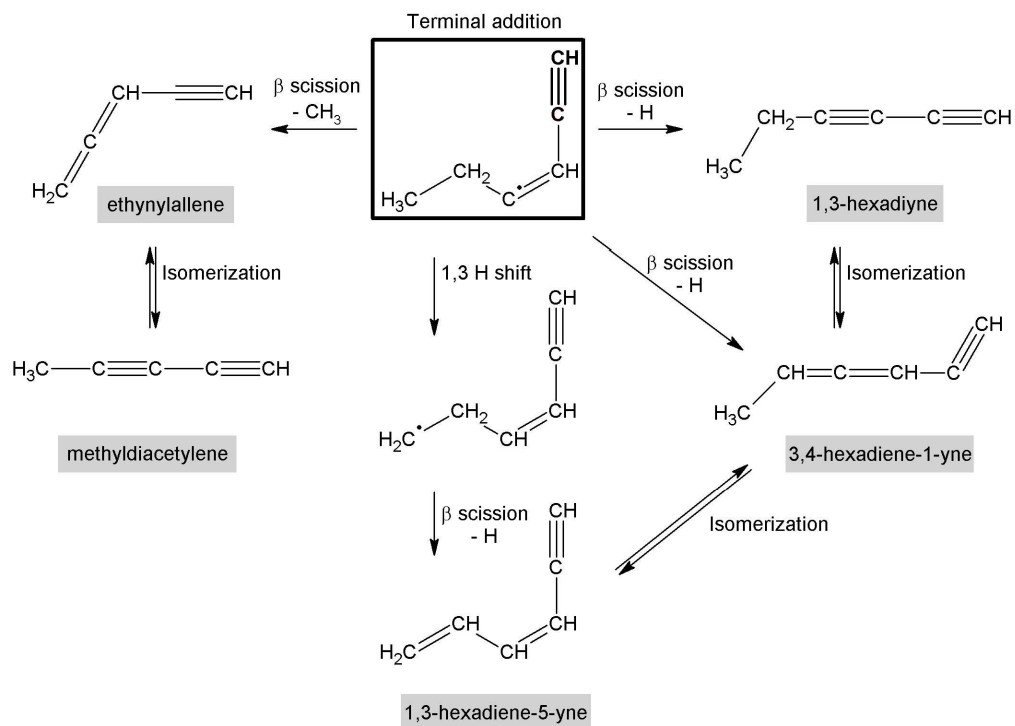
143x140mm (300 x 300 DPI)



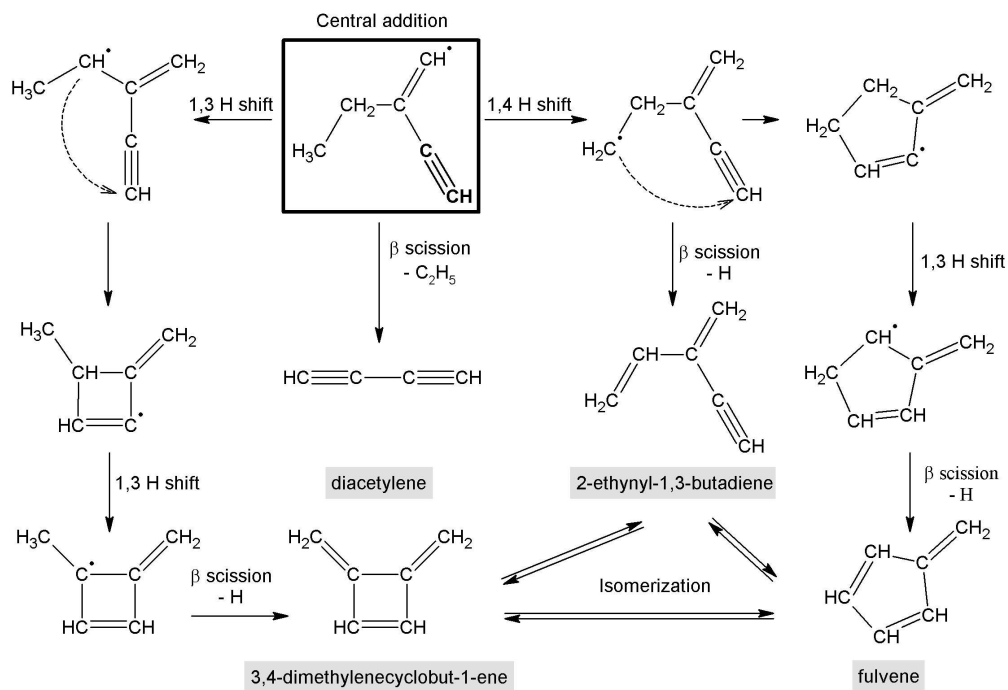
202x145mm (300 x 300 DPI)



226x149mm (300 x 300 DPI)



176x127mm (300 x 300 DPI)



189x128mm (300 x 300 DPI)